Identification of Pesticides Using Experimental and Computational Approaches based on Ion Mobility Mass Spectrometry Measurements

by

Benedicta Donkor

A thesis submitted to the Graduate Faculty of
Auburn University
in partial fulfillment of the
requirements for the degree of
Master of Science

Auburn, Alabama
August 6, 2022

Keywords: mass spectrometry; ion mobility; collision cross section; degradation products; precursor pesticides

Approved by

Hamid M. Ahmed, Chair, Assistant Professor of Chemistry and Biochemistry
Christopher J. Easley, C. Harry Knowles Professor of Chemistry and Biochemistry
Steven Masoorabadi, J. Milton Harris Associate Professor of Chemistry and Biochemistry

Abstract

Mass spectrometry is known to be a powerful analytical technique due its high sensitivity, specificity, speed, and versatility. It has the capability of detecting and identifying numerous analytes in sample matrices. In addition, several complementary techniques have been coupled to mass spectrometry for improved analyte identification such as chromatography and ion mobility. This thesis focuses on (i) synergistic experimental (LC-MS/MS) and computational (DFT calculations) studies on the fragmentation pattern of two types of organophosphate pesticides for the prediction of possible degradation products. (ii) identifying pesticides and degradation products using experimental approaches; liquid chromatography ion mobility mass spectrometry (LC-IM-MS) and paper spray ion mobility mass spectrometry (PS-IM-MS) and supporting the experimental findings with theoretical calculations. Tandem liquid chromatography-mass spectrometry (LC-MS/MS) is typically utilized in the analysis of pesticides and degradation products. However, this technique is costly and time consuming. Also, some degradation products (which are often overlooked during screening of pesticides in food) of pesticides are reported to be more harmful than the parent pesticides. Hence, there is a need for rapid and efficient techniques for the screening of pesticides, and their degradation products in agricultural produce. Isomeric and non-isomeric parent pesticides and their degradation products were screened using LC-IM-MS. Due to time constraints of the LC method (time-consuming), an alternative rapid method, PS-IM-MS, was employed for the screening and identification of the analytes using their accurate mass measurements and collision cross-section values. The ion mobility separation method was utilized to investigate structures of parent pesticides and their corresponding degradation products. The structures were identified by comparing the measured collision cross section values with those predicted from DFT computations.

Acknowledgements

First and foremost, I am grateful to God for the gift of life. I am forever grateful to my supportive parents, Mr. Samuel Donkor and Mrs. Selina Donkor as well as my loving siblings, David, Rebecca and Hadassah. I am blessed to have them as part of my life journey. I would like to thank my advisor, Dr Ahmed. M. Hamid for his guidance from the beginning to the completion of my project. I am also grateful to my research advisory committee members, Drs. Christopher Easley, and Steven Mansoorabadi for their kind and meticulous advice. Sincere thanks to Dr. Angela Calderon for her contribution towards my academic journey.

Additionally, I would like to thank our group members for their contributions, great times, and workable environment. I am also grateful to Joe Baudailler and Dawn Stickle (Agilent Technologies) for their advice and help. Sincere thanks to Viraj Ghandhi, and Dr. Carlos Larriba-Andaluz, (Purdue School of Engineering and Technology) for the valuable discussions regarding computational studies. Earnest appreciation to my professors in the department of Chemistry, Kwame Nkrumah University of Science and Technology, Drs Akwasi Acheampong, Marian Asantewah Nkansah, Richard Tia, Nathaniel Owusu Boadi, and Eric Agorku, for their candid advice and recommendations. My heartfelt gratitude to all house fellowship and Pentecost members who have been more than a family to me in the USA. I express my sincere gratitude to my friends and/or colleagues Ernest, Rashid, Stella, Katie, Kathy, and Aaron for being very supportive in diverse ways. I appreciate each and every one who has directly or indirectly contributed to my education in numerous dimensions.

Dedication

This work is dedicated to the Donkor, Bevard and Bonafede families. I am forever grateful for their love and support.

TABLE OF CONTENTS

List of Figures

List of Tables

List of Abbreviations

ACN – Acetonitrile
AFADESI – Airflow assisted desorption electrospray ionization
APCI – Atmospheric pressure chemical ionization
APPI – Atmospheric pressure photoionization
CBS – Coated blade spray
CCS – Collision cross section
DEA – Atrazine-desethyl
DESI – Desorption electrospray ionization
DFT – Density functional theory
DIA – Atrazine-desisopropyl
DTIMS – Drift tube ion mobility spectrometry
EI – Electron impact
ELDI – Electrospray-assisted laser desorption/ionization
ESI – Electrospray ionization
FAIMS – Field asymmetric ion mobility spectrometry (FAIMS)
GC-MS – Gas chromatography mass spectrometry
HDPE – High-density polyethylene
HPLC – High-performance liquid chromatography
IM – Ion mobility
IMP – 2-Isopropyl-6-methyl-4-pyrimidinol
IT – Ion trap
LC-IM-MS – Liquid chromatography mass spectrometry
LC-MS – Liquid chromatography mass spectrometry
LC-MS/MS – Tandem liquid chromatography mass spectrometry
MALDESI – Matrix assisted laser desorption electrospray ionization
MALDI – Matrix-assisted laser desorption ionization
MS – Mass spectrometry
MS – Mass Spectrometry
Ops – Organophosphates
PS-IM-MS – Paper spray ion mobility mass spectrometry
PS-MS – Paper spray mass spectrometry
QqQs – Triple quadrupole analyzers
QTOF – Quadrupole time of flight
RT – Retention time
SPE – Solid phase extraction
TCP – 3,5,6-Trichloro-2-pyridinol
TOF – Time of flight
UHPLC – Ultra high-performance liquid chromatography

1.0 **Introduction**

1.1 Mass spectrometry

Mass spectrometry (MS) is an analytical tool used for the measurement of mass-to-charge ratio of molecules in a sample. A mass spectrometer consists of four separate sections irrespective of the instrument type; inlet system, ion source, mass analyzer, and detector.[1] An inlet is required to transfer sample from ambient room temperature and pressure into the ion source since the mass spectrometer operates in vacuum. The sample is converted to ions in the ion source and separated based on their mass-to-charge ratio. The separated ions are detected (by the detector) and recorded. MS has been utilized in diverse fields for numerous analysis. For instance, in the 1940s mass spectrometers were used in the analysis of the abundance of small hydrocarbons in the petroleum industry.[2] From the 1960's, chemists from diverse fields began to explore the use of the mass spectrometer to fragment molecules and better obtained insight of its various applications.[2] In the analysis of doping agents, MS was utilized in the late 1960's and its usage in these type of analysis increased over the years.[3] Currently, MS is known as one of the most rapid, sensitive, specific and versatile techniques.[4] It has been coupled to several prior separation methods like gas chromatography (GC), liquid chromatography (LC), and ion mobility (IM) for enhanced separation and identification of analytes. Also, it is coupled to various ionization techniques like atmospheric pressure chemical ionization (APCI), paper spray ionization, electron impact (EI), atmospheric pressure photoionization (APPI), electrospray ionization (ESI), matrix-assisted laser desorption ionization (MALDI), and desorption electrospray ionization (DESI) among others.

1.1.1 Liquid Chromatography Mass Spectrometry

The coupling of LC with MS became a rigorous subject of investigation after both analytical techniques gained acceptance.[5] The hyphenation of GC and MS with an EI interface was a success as a good deal of fragmentation was observed in the spectra obtained, which was proven to be highly reproducible. LC-MS was difficult to realize than GC-MS due to the presence of the liquid solvent. The vacuum system was burdened with the responsibility of removing large amounts of solvents even when volatile solvents are in use.[5] Due to this, intensive efforts were put into obtaining more efficient vacuum pumps for LC-MS than that of GC-MS. When turbo-molecular pumps were replaced with oil-diffusion pumps, the challenge of maintaining a sufficient level of vacuum was partly solved. Another drawback was that heavier non-volatile analytes were difficult to ionize and analyze. Cleaning of ion sources due to contamination from sample matrices and contaminants from solvents was tedious and time-consuming. There has been improvement over the years in this technique to address the aforementioned problems.[5-6] In the LC, compounds are separated based on their polarity.[7] Compounds that have a higher affinity for the stationary phase elute later compared to compounds with less affinity for the stationary phase. Likewise, compounds with higher affinity for the mobile phase elute faster compared to compounds with less affinity. The ions of the separated compounds are then identified using mass spectrometry. Various mass analyzers such as single quadrupole, triple quadrupole (QqQs), ion trap (IT), orbitrap, and quadrupole time of flight (QTOF) or time of flight (TOF) among others can be coupled to the LC. The development of tandem liquid chromatography mass spectrometry (LC-MS/MS) has skyrocketed for the analysis of numerous complex samples. LC-MS/MS is mostly used in the routine screening of pesticides in food, blood and urine.[8] It has also been employed successfully

in the analysis of chemical warfare agents[9], mycotoxins[10], illicit drugs[11], and pharmaceuticals[12] among others.

1.1.2 Ion Mobility Mass Spectrometry

In spite of the success with LC-MS/MS, there is difficulty in using this technique to differentiate between some isomeric pesticides which are currently in use.[6] In the LC-MS/MS technique, the precursor pesticide ions are selected for fragmentation. The fragmentation patterns obtained are used for the identification of the analytes by comparisons to established databases. A previous study reported that, some isomers have similar fragmentation patterns hence cannot be differentiated using this technique.[13] Ion mobility (IM) is a gas phase technique that separates ions according to their size, shape, mass, and charge. There are four ion mobility separation methods currently in use; i. drift tube ion mobility spectrometry (DTIMS), ii. traveling wave ion mobility spectrometry (TWIMS), iii. aspiration ion mobility spectrometry (AIMS), and iv. field-asymmetric waveform ion mobility spectrometry (FAIMS) which is also called differential-mobility spectrometry (DMS).[14] For the purpose of this thesis, a special focus on the operation of DTIMS is given due to its direct application. DTIMS is made up of a series of stacked-ring electrodes with a near uniform electric field applied along the axis of the drift tube and an introduced buffer gas.[15] Ions formed are accumulated and stored in the trapping funnel and released in ion packets into the drift tube. The electric field is used to move the ions forward while the buffer or neutral gas retards the forward movement of the ions. The ions move at constant velocity, proportional to the electric field, while any energy gained from the electric field is dissipated by collisions with neutral molecules of the drift gas.[15]

IM separates compounds within milliseconds. Based on the interactions of the ions with the carrier gas in the drift tube, the ions may have different arrival times and their corresponding collision cross-section (CCS) values accordingly determined that can act as unique molecular descriptors.[16] The various CCS values of the compounds obtained from IM are unique to the structure of the analyte hence can be used to differentiate between isomers. Ions move through a buffer gas in the drift tube by the application of a gradient voltage or electric field. The ions are decelerated by the collisions with a buffer gas. The drift velocity of the ion is determined by the ratio of the distance the ions travel through the drift tube to the time spent to get to the detector (Eq.1.1).[17]

$$v_d = \frac{\mathrm{L}}{\mathrm{t}_d} \tag{1.1}$$

where L is the distance and t_d the drift time of the ion. The mobility of the ion (K) is determined by the ratio of the ion's drift velocity to the applied electric field (E) as shown in equation 1.2.[17]

$$K = \frac{\mathrm{v_d}}{\mathrm{E}} \tag{1.2}$$

Factors such as temperature and pressure of the drift tube affects the drift velocity hence K is normalized to standard temperature and pressure conditions of 273K and 760 torr (Eq. 1.3).[17]

$$K_o = K * \left(\frac{273.15}{\mathrm{T}}\right)\left(\frac{\mathrm{P}}{760}\right) \tag{1.3}$$

CCS can be calculated using the Mason Schamp equation.

$$K = \frac{3}{16}\frac{\mathrm{q}}{\mathrm{N}}\left(\frac{2\pi}{\mu \mathrm{kT}}\right)^{1/2}\frac{1}{\Omega} \tag{1.4}$$

A combination of E/N governs the movement of the ion in the drift tube. Equation 1.4 holds at low electric field limit where the ratio of E/N is small (N is the number density of buffer gas).[17] When E/N is small, the energy gained by the ion from the electric field is considered negligible because collisions with molecules of the buffer gas dissipates any field-acquired energy.

The ratio of E/N is reported in townsend (Td, 1Td = 1×10^{-17} Vcm^2) when E is in volts and N in particles/cm^3. Hence one townsend can be calculated using equation 1.5.[17]

$$Td = \frac{\mathrm{E}}{\mathrm{N}} * 1 \times 10^{17} \quad (1.5)$$

There is variability in the reduced mobility of an ion as a function of the buffer gas pressure and electric field through which the ions move. The mobility of an ion as a function of Td can be described in regards to low field conditions where mobility is constant. Drift tube ion mobility spectrometry (DTIMS) operates under these conditions. To this end, the mobility coefficient is independent of E/N as the energy gained from the electric field by the ion is negligible.[18] The reduced mobility is therefore constant.

CCS values can be calculated using two different methods: stepped-field[19] and single-field[20]. In the stepped-field approach (only calibrant-independent method), multiple drift fields (usually a minimum of six electric fields) are utilized for the estimation of CCS values by building a linear regression curve between the measured arrival times and the inversed drift voltages.[21] The time the ions spend outside the drift tube (i.e. in MS) is obtained from the y-intercept. The corrected ion mobility drift time is obtained by subtracting the time spent outside the drift tube from the uncorrected drift time which is then utilized for CCS calculation using the Mason Schamp equation. In step field measurement, accurate CCS values are obtained due to the direct attainment of the CCS values (no calibrant required for the calibrant).[21b] Hence there is no effect of the calibrant on the analyte measurement when calibrant is not similar due to different physical properties and gas-phase conformations of calibrant from analyte of interest.[22] Some of the limitations associated with this method include the use of large volumes of samples, more analysis time needed and the inability for prior separation techniques (such as coupling LC or GC before IM) when complex samples are utilized. In contrast to the multiple drift fields used in stepped-

field, a single drift field is used to measure the CCS values in the single-field method. Typically, Agilent tune mix ions (a mixture of mobility calibrants) are used in acquiring single-field measurements due to their known CCS values. The calibrants are used to create a linear calibration curve between the arrival times of the ions and their corresponding CCS values. The obtained calibration curve allows the experimental CCS values of the analytes to be obtained from their arrival times.[20a] Due to the orthogonality of the different separation techniques involved when IM is coupled to LC-MS, it offers an enhanced approach for the identification of pesticides and their degradation products.[23] It benefits from additional descriptors collectively used to determine the CCS values in addition to retaining m/z and retention times for easy compound identification.

1.2 Ambient Ionization

Different analytical techniques, including immunoassays (IAs)[24], mass spectrometry (MS) coupled to GC or high-performance liquid chromatography (HPLC), liquid chromatography-ultraviolet detection[25], and others, have been developed for the analysis of various complex samples. Ambient ionization methods are new approaches pertinent to the direct analysis of samples in their ambient states, followed by mass spectrometric analysis[26]. Ambient ionization techniques have been used to ionize samples directly from papers, leaves, needles, etc. The origin of ambient ionization could be ascribed to the electrospray ionization (ESI) developed by Fenn and coworkers[27] which was further developed by Cooks et al.[28] Cooks and colleagues developed desorption electrospray ionization (DESI), a special ambient ionization source based on electrospray ionization (ESI) to overcome complex matrix interference in ESI.[28] Ambient ionization techniques, such as direct analysis in real time (DART)[29] and DESI[28] avoid sample preparation by directly ionizing the analyte from the sample for analysis using mass spectrometry.

These techniques have increasingly developed and proven to act as potentially valid high throughput analytical techniques.[30] Over the years, many ambient ionization techniques have been developed for numerous analyses. Some of these techniques include airflow assisted desorption electrospray ionization (AFADESI), coated blade spray (CBS), electrospray-assisted laser desorption/ ionization (ELDI), touch spray, matrix assisted laser desorption electrospray ionization (MALDESI), etc.[31] Ambient ionization has been applied in diverse fields ranging from environmental, clinical, and petroleum among others to solve many problems.[31-32]

1.2.1 Paper Spray Mass Spectrometry

An alternative for the direct analysis of analytes in samples is using paper spray mass spectrometry (PS-MS). As described by Wang et al.,[33] paper spray is an ambient ionization technique in which a solid or liquid sample is applied onto the surface of a cellulose or semi-cellulose material (paper substrate). A triangular sharp edge paper is cut pre- or post-sample application and the pointed tip is positioned in front of the mass spectrometer inlet (typically 3-10 mm away). Spray solvent is applied to the paper where it interacts with the sample and extracts the analytes. The size and properties of the paper (like thickness and porosity) used play a role in determining the solvent volume to use. Utilizing excessive amount of the solvent, will lead to solvent pooling underneath or running off the paper hence causing spray signal instability resulting in lower MS signals. When a high voltage is applied to the paper (usually in 3-5 kV range), ESI is instigated from the tip of the paper.[34] Upon arrival to the tip of the paper positioned in front of the mass spectrometer inlet, electrospray occurs, and the resulting ions are detected with mass spectrometry.[33-34] PS is a technique with minimal sample preparation requirements and has been shown to be usable to detect analytes quantitatively at low concentration levels.[33-34] [35] Due to its advantages of rapid analysis

and low-cost, its usage in the analysis of numerous compounds in biological tissues,[36] chemical warfare agents,[37] urine,[38] have been reported. Leaf spray[39], wooden tip spray[40] porous polymer tip spray[41], metal needle spray[42] and fiber spray[43] are other available ambient ionization sources with similar principles of operation to paper spray.

Matrix effects cause limitations in the detection limits when PS-MS is used. In the absence of any separation technique or sample cleanup step before analyzing samples using MS, there is poor analyte recovery and ion suppression which leads to an increase in the detection limits of analytes.[34] Recently, studies on improving detection limits of PS-MS have been demonstrated.[35c, 44] Some factors are to be considered in PS-MS since they can bring about bias in results.[38, 45] These factors may instigate a decrease or increase in analyte signal thereby causing a false positive or negative result. Paper substrate (paper composition), solvent, sample position (i.e., moving sample farther or closer to the spray tip), paper holder, and matrix are approaches that were found to be impactful. Most often, alligator clips and paper cartridges are used in holding the substrate at the inlet of the mass spectrometers.[45b, 46] Most automated paper cartridges are made by plastic using 3D printing which is one of the affordable means for fast prototyping devices for MS.[47] The starting material of these cartridges which are plastics can be deleterious in the sense that they could leach contaminants or bind to analytes, resulting in ionization enhancement or suppression which would lead to bias results. There is a major concern since the printed material makes direct contact with the organic solvents in use. There can be deformation or dissolving of the plastic due to chemical interaction.[48] Zhang and Manicke[44b] employed solid-phase extraction to selectively concentrate target analytes while removing some of the matrices. Compared to direct analysis, mass spectra using the SPE cartridge exhibited a higher signal-to-noise (S/N). Furthermore, various research have innovated the modification of the paper substrates to improve analyte

sensitivity. Damon and comrades utilized a silanization reagent (Trichloro(3,3,3-trifluoropropyl)-silane) to treat the paper in order to increase the sensitivity of analytes which is similar to a recent work by Rossini and his team.[38]

Vega and coworkers[49] reported that ion recovery and suppression were both matrix- and compound-dependent. Poor ionizers (e.g., analytes lacking basic aliphatic amine groups) had the highest levels of ion suppression while there was little or no suppression for good ionizers (analytes with aliphatic amines) in a blood sample. Yannell et al.,[50] studied the effect of matrix on signal intensity and reported that the lower overall signal for the internal standard (IS) in whole blood is caused by ion suppression and from recovering less sample due to the physical barriers on the paper from the matrix. Based on the progressing development made in PS, its usage and implementations has spread across many areas. There is an increasing trend of evaluating paper spray's ability to be applied in many fields such as analysis of phytochemicals in plants[51], pharmaceutical drugs[52], biological samples[53], quality of foodstuff[53-54], gasoline[55], chemical warfare agents[37], rapid evaluation of illicit drugs and pesticides in foodstuff[56].

1.2.2 Paper Spray Ion Mobility Mass Spectrometry

PS-MS has been used successfully for the screening of pesticides in food matrices and analysis of various analytes.[57] However, there is difficulty in differentiating between geometric isomeric pesticides due to the same m/z ratio. When IM separation is incorporated into PS-MS, i.e. forming PS-IM-MS, it would make separation, selectivity and identification of analytes (especially isomers) using this approach more effective. An experimental setup for the PS-IM-MS is shown in Scheme 1.1. A study by Manicke and Belford[58] utilized field asymmetric ion mobility spectrometry (FAIMS) to improve selectivity by separating opiate isomers in mass spectrometric

analyses. The separation of the opiate isomers: morphine, norcodeine, and hydromorphone which are similar in structure was achieved, but required configuring the FAIMS for maximum resolution. Also geometric lipids and constitutional isomers were separated and identified using PS coupled to a commercial drift tube ion mobility mass spectrometry instrument in our laboratory.[59] PS-IM-MS offers an enhanced approach to the identification of compounds.

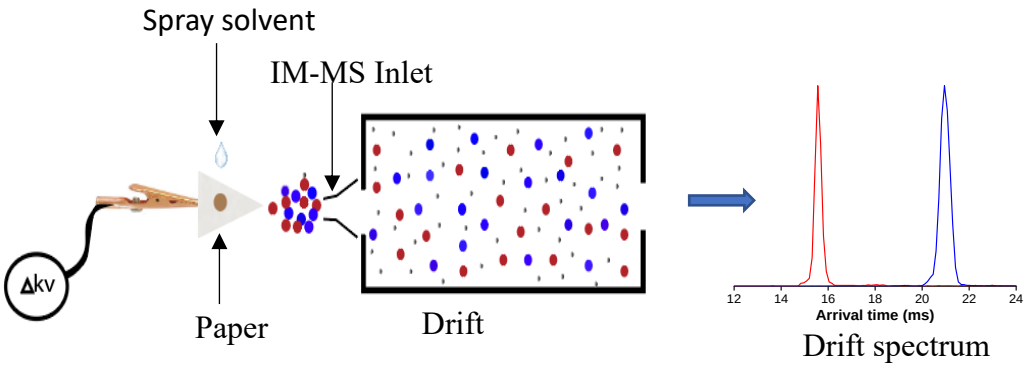

Scheme 1.1: Analysis of a sample by paper spray ion mobility mass spectrometry

2.0 **Prediction of fragmentation patterns of pesticides: Application to organophosphate pesticides analysis**

2.1 Introduction

Organophosphates (OPs) present a class of pesticides often used in agricultural settings after the ban of most organochlorine pesticides[60] (owing to their higher toxicity levels and expensive waste management).[61] In fact, majority (~40%) of pesticides that are produced and used commercially belong to OPs category.[62] OPs are extensively used because they are relatively cheaper, have low persistence nature in the environment, and are used to destroy many pests.[63] However, it is reported that the majority of these pesticides are highly toxic.[63-64] Humans are exposed to truncated levels of OPs mainly through ingestion (diet), inhalation (through the air), and dermal adsorption (contact with the body).[62] A study evaluated the effect of OPs on the spouses of farmers who applied organophosphate pesticides.[65] It was indicated that hormonally related cancers were consistent with the popular notion that OPs are endocrine disruptors. Exposure to OPs has been linked to neurotoxic disorders[66] and traits related to autism spectrum disorders.[66a] Malathion, diazinon, dimethoate, and chlorpyrifos are among the most commonly used organophosphates registered by the Environmental Protection Agency (EPA) of the United States.[67] A recent study showed that exposure to diazinon[68] could be a possible cause of breast cancer in females. Jaga and Dharmani reported that the exposure to OPs, particularly malathion, led to an ocular disease known as the Saku disease.[69] This condition was found to be associated with features such as, astigmatism, abnormal eye movement, reduced vision, and myopia. Also, over 3 million people are exposed to OPs annually and experience unintentional pesticide poisoning with 300,000 mortalities.[62] Due to the aforementioned problems associated with exposure to OPs, it is important to understand their fragmentation pathways that provide molecular-level insights which will be beneficial for the collective regulation of OPs. The

degradation of OPs occurs through several processes such as oxidation, hydrolysis, desulfuration, etc in diverse environments (soil, atmosphere, fruits, and vegetable among others). Also, the pH of the media in which the OPs are present in (acidic or basic) and the presence or absence of sunlight among others contribute to their degradation. It is reported that some of the degradation products are more toxic than the parent pesticides, hence, can result to serious health problems. For instance, it has been reported that dimethoate undergoes desulfuration to produce more toxic omethoate, which can induce cholinergic crisis and eventually lead to death.[70] Hence, the unintentional OP poisonings aforementioned may not only be related to the parent pesticides but also some of the degradation products which are toxic. Some of the degradation products of OPs are widely known together with their toxicity while some remain unknown. The requirement to systematically uncover the possible health effects of OPs so as to minimize their toxicological side effects has increased rapidly.[71] Hence it is important to detect more degradation products in trace amounts and to know their toxicological effects in order to help generate new approaches to degrade the pesticides to form less toxic or neutral compounds.

In analytical techniques, fragment ions are conventionally determined through LC-MS/MS experiments. LC-MS/MS makes use of the precursor ion mass-to-charge (m/z) ratio and their corresponding retention times for fragmentation. Some of these fragment ions obtained experimentally can be compared to degradation products or metabolites of the parent pesticides through fragmentation/degradation relationships.[72] Recent literature reveals that fragment ions of an analyte could be predicted through computational calculations.[73] John *et al*[70] reported synergistic experimental and computational studies on the fragmentation pathways of dimethoate and omethoate generated by electrospray ionization. In their work, density functional theory (DFT) computation was utilized to produce a set of concise data for the complementary identification of

dimethoate and omethoate product ions. When a better insight on how the fragmentations of OPs occur at the molecular level is obtained, it would be easier to elucidate the structure of several degradation products in order to test their level of toxicity to avoid unintentional OPs poisoning which may take effect after degradation of the parent pesticides.

In this work, LC-MS/MS experiment was conducted on two different types of OPs; malathion and dimethoate (S=P-S, type 1), chlorpyrifos and diazinon (S=P-O, type 2) to obtain their fragmentation patterns.[74] At the same time, the plausible fragment ions anticipated from the said OPs were predicted through computational calculations. Computational calculations were used to suggest the most stable protonation sites of the selected pesticides and to calculate changes in the diverse bond lengths after protonation to confirm favorable fragmentation sites. Basic sites of the aforementioned pesticides were selected based on natural bond orbital (NBO) analysis, protonated individually and the optimized geometry of each ionic species determined.[70] Data from the DFT calculations are discussed in light of the experimental findings from LC-MS/MS. The difference in the fragmentation pathway to obtain similar fragment in the experiment (by the two types of OPs) was also highlighted. In addendum, Metfrag was utilized in conjunction with the DFT calculations for better insight into how the fragmentations occur at the molecular level.[75]

2.2. Experimental and Theoretical Methods

2.2.1 Chemicals and Equipment

Chlorpyrifos, dimethoate, malathion, and diazinon standards were purchased from Sigma-Aldrich. High purity solvents: formic acid, acetonitrile, and ultra-pure water (H_2O) were purchased from Agilent Technologies (Santa Clara, CA), and were used throughout the duration of the experiment. A commercial Agilent 6560 IM-QTOF (Agilent Technologies, Santa Clara) system equipped with

Agilent jet-stream (AJS) was used. An Agilent 1290 Infinity II (HPLC) which comprises of a binary pump, multi-sampler, and a heated column compartment was utilized. Data was acquired using Agilent's MassHunter acquisition software (version B.09.00) and processed using Qualitative Analysis 10.0 (Agilent). Graphs and plots were generated using Origin version 2018b (64-bit) b9.5.5.409 (Academic).

2.2.2 Instrument Operation Settings

Liquid chromatography measurements were performed using Agilent Infinity Poroshell 120 EC-C18, 2.1 x 50 mm, 1.9 µm (p/n 699675-902) at a flow rate of 0.4 ml/min, column temperature 45 ^{o}C, and a pressure limit of 1200.00 bar. The injected sample volume was 10 µl for all experiments. An isocratic method of H_2O-ACN (98:2, v/v) was used from time t=0 min to t=1 min, then H_2O-ACN gradient (71:29, v/v) at time t=2.5 min, (66:34, v/v) at time t=4 min, (10:90, v/v) at time t=10.5 min, and (2:98, v/v) at time t=11 min was used with a post run time of 2 min. Mobile Phase A comprised of 0.1 % formic acid in ultra-pure H_2O and mobile phase B was ultrapure ACN. Needle wash: 1:1:2 H_2O/ isopropyl alcohol (IPA)/MeOH. All experiments were performed in the positive mode. Gas temp. 325 ^{o}C, gas flow 5 l/min, nebulizer 35 psi, sheath gas temp. 275 ^{o}C, sheath gas flow 11 l/min, capillary voltage 3500 V, nozzle voltage 1000 V, fragmentor 400 V. The acquisition rate was 1 spectrum/sec. For the MS/MS experiments, wide, medium, and narrow isolation widths were assessed where the narrow isolation window was chosen for the experiments for enhanced specificity. Collision energies (CEs) of 0 to15 eV were varied at 5 eV increment for all the precursor ions and 5 eV spectra was selected for malathion and dimethoate while 15 eV and 10 eV respectively were selected for diazinon and chlorpyrifos for presentation purpose. These (CEs) for the various presented spectra were chosen based on visual inspection of relevant

fragment ions with high intensity of fragment ions and minimum intensity of parent ion. The chosen CEs gave a fair representation of the fragment ions observed in the various pesticide ions.

2.2.3 Preparation of standard solution

1mg/mL (1000 ppm) stock solutions of chlorpyrifos, malathion, dimethoate, and diazinon were prepared in ultra-pure ACN. 10 ppm working solution was prepared from the stock solution and diluted to 10 ppb using 75% ACN except for chlorpyrifos where H_2O was used for dilution.

2.2.4 Computational Details

DFT calculations were carried out using the Gaussian 16 software package.[76] Geometry optimization and vibrational frequency analysis were performed at B3LYP/6-31G(d,p) level of theory. A zero-point energy correction was performed for all calculated structures. Basic sites of the pesticides were selected based on NBO analysis, protonated individually and the optimized geometry of each ionic species determined. The protonation sites are labeled as sites A1-A8 in Figures 2.1 a to d respectively for malathion, dimethoate, diazinon, and chlorpyrifos. Bond lengths of the atoms were compared before and after the protonation of the pesticides.

2.2.5 Atomic charges and protonation site selection

NBO analysis is a tool that facilitates the interpretation of electronic structure calculations in a chemically intuitive manner.[77] Figure 2.1a-d displays the numbering of the more negative atoms in diazinon, chlorpyrifos, propazine, and terbuthylazine while Table 2.1 displays their NBO atomic charges at B3LYP/6-31G(d,p) level of theory. The possible protonation sites were selected based on the NBO analysis. The structure with the lowest energy was selected as the most stable structure. Bock et al[78] selected the protonation sites of both N-(6-methoxypyridin-3-yl)-4-(pyridin-2-yl)thiazol-2-amine mono-hydrobromide monohydrate and N-(6-methoxypyridin-3-yl)-

4-(pyrazin-2-yl)thiazol-2-amine mono-hydrobromide based on the difference in electron density provided after NBO calculations where the atoms with the negative natural atomic charge were selected for the protonation sites of the cations.[79] From the results, the atoms listed in Table 2.1 were selected for protonation due to their possession of more negative atomic charges hence are likely protonation sites.

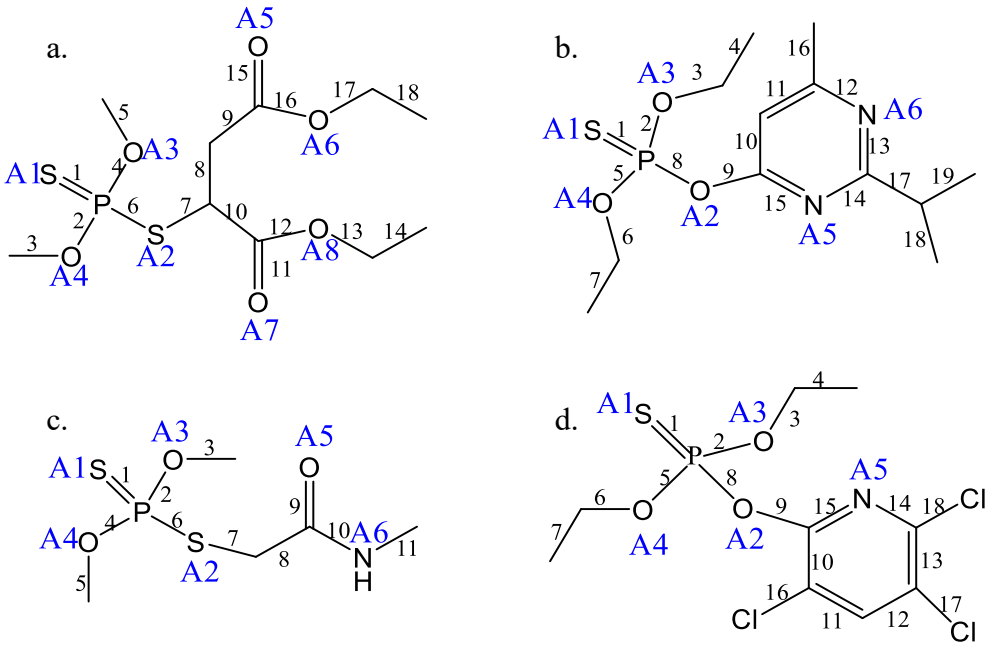

Figure 2.1: Structures of OPs considered in this work and their bond labels a. Malathion b. Diazinon c. Dimethoate d. Chlorpyrifos

Table 2.1: NBO charge distribution of parent pesticides (diazinon, chlorpyrifos, propazine, and terbuthylazine

Possible protonation site	Malathion	Diazinon	Dimethoate	Chlorpyrifos
	NBO Charge Distribution			
A1	-0.542	-0.584	-0.545	-0.571
A2	-0.046	-0.787	-0.064	-0.777
A3	-0.846	-0.858	-0.846	-0.859
A4	-0.849	-0.845	-0.847	-0.843
A5	-0.615	-0.546	-0.622	-0.484
A6	-0.551	-0.517	-0.666	
A7	-0.586			
A8	-0.539			

2.2.6 MetFrag Analysis

Metfrag web version 2.4.6 was utilized for the analysis of the fragment ions.[75] PubChem was utilized as a database. The molecular formula, neutral mass, and precursor ion mass were used to retrieve the possible structure candidates in the positive ion mode. After retrieving possible candidates, fragment ions from MS/MS experiment were typed into the MS/MS peak list in the fragmentation settings and processing section. Also, 5 ppm mass accuracy, 0.001 absolute intensity, and positive mode were selected. Candidates were processed at this stage. The identifier IDs were compared to that at PubChem to select the right analyte. The theoretical fragment ions are compared with the corresponding experimental fragment ions based on their accurate mass measurements and score. Qualified fragment ions were labeled as matched while unqualified ones were labeled as unmatched.

2.3 Results and Discussion

2.3.1 Fragmentation of Organophosphate Pesticides

In this work, fragmentation patterns of organophosphate pesticides (dimethoate, diazinon, malathion, and chlorpyrifos) were obtained using LC-MS/MS. The fragmentation patterns were utilized for the confirmation of the identity of the analytes. DFT was extensively used for the simulation of chemical structures and has been previously described in section 2.2.4.[70, 80] Theoretical calculations were performed on the analytes to obtain better insights into how these fragmentations occur. Changes in bond length and relative energies were calculated for all the selected possible protonation sites.

2.3.2 Search for stable protonation sites for the selected OPs

Malathion: After geometry optimization of the possible protonation sites, proton transfer from A4 to A7 (see Figure 2.1) was observed. Hence the structure protonated at A4 converged to a similar structure as A7 with the most stable relative energy of 0.0 kcal/mol (Table 2.2). For the original structure protonated at A7, the obtained relative energy is found to be 0.97 kcal/mol. Hence it can be said that the most stable protonation site for malathion was at A7. Similar proton transfer was observed in a previous study where there was proton transfer from an oxygen atom in methoxy to the carbonyl oxygen in an omethoate structure.[70] In their study the most stable structure for omethoate was found to be the one protonated at the carbonyl oxygen. This indicates the availability of the carbonyl oxygen to readily accept protons in the structure.

Diazinon: Two relatively stable protomers were observed for diazinon structure with relative energies of 0.0 kcal/mol and 0.2 kcal/mol. These two stable protomers were protonated at the two N atoms on the pyrimidine ring. This indicates that the N-atoms in the structure were the basic sites that were readily available to accept the protons. This agrees with a previous study that reported that the protonation sites in diazinon that are thermodynamically favorable are the N atoms in the pyrimidine structure.[81]

Dimethoate: Protonation at A3 revealed a structure which converged to a structure similar to the one protonated at A5 with 0.0 kcal/mol relative energy. This also reveals proton transfer from the oxygen in the methoxy to the carbonyl oxygen as observed earlier in malathion. Hence A5 was the most stable obtained protonated structure.

Chlorpyrifos: Proton transfer was also observed in the plausible protonated sites of chlorpyrifos after geometry optimization. It was observed that there was proton transfer from A3 (oxygen in methoxy) to A5 (the N atom) hence A3 converged at A5 with relative energy of 1.8 kcal/mol. The

most stable protomer was protonated at the N atom which indicates the nitrogen atom in the pyridinyl structure is the most favorable protonation site in chlorpyrifos (most basic site).

Table 2.2: Absolute energies of protonated and non-protonated malathion and their respective relative energies (kcal/mol)

Protonation site	Malathion	Diazinon	Dimethoate	Chlorpyrifos
A1	11.00	16.82	8.88	7.17
A2	26.35	40.43	26.92	30.52
A3	8.23	36.13	0.00	1.80
A4	0.00	8.82	28.19	23.35
A5	13.05	0.17	1.06	0.00
A6	9.26	0.00	15.07	
A7	0.97			
A 8	23.32			

2.3.3 Rationalization of experimental data using computational studies

Numerous cases of OP pesticide poisoning[62] may not only be related to the parent pesticides but also some of the degradation products which are harmful (sometimes more toxic than the parent pesticide).[70, 72, 82] Some degradation products of pesticides, and their toxicity levels are known while others may not be known due to less focus on them. In this section, the synergistic experimental and theoretical calculations data are discussed. Fragmentation patterns observed in experiment can be compared to degradation products or metabolites of the parent pesticides through fragmentation/degradation relationship.[72] Hence it can be said that, most of the fragment ions observed in experiment are possible degradation products or metabolites of the parent pesticide. Regarding this, the fragmentation patterns observed experimentally are discussed below in light of the computational findings.

2.3.3.1 Fragmentation of malathion

Fragmentation of the precursor ion revealed fragment ions with accurate mass measurements 285.0011, 257.00557, 158.9696, 124.98143, 127.0391, and 99.0079 (Figure 2.2a). The experimental fragmentation patterns are discussed below and supported with the finding from the computational calculations.

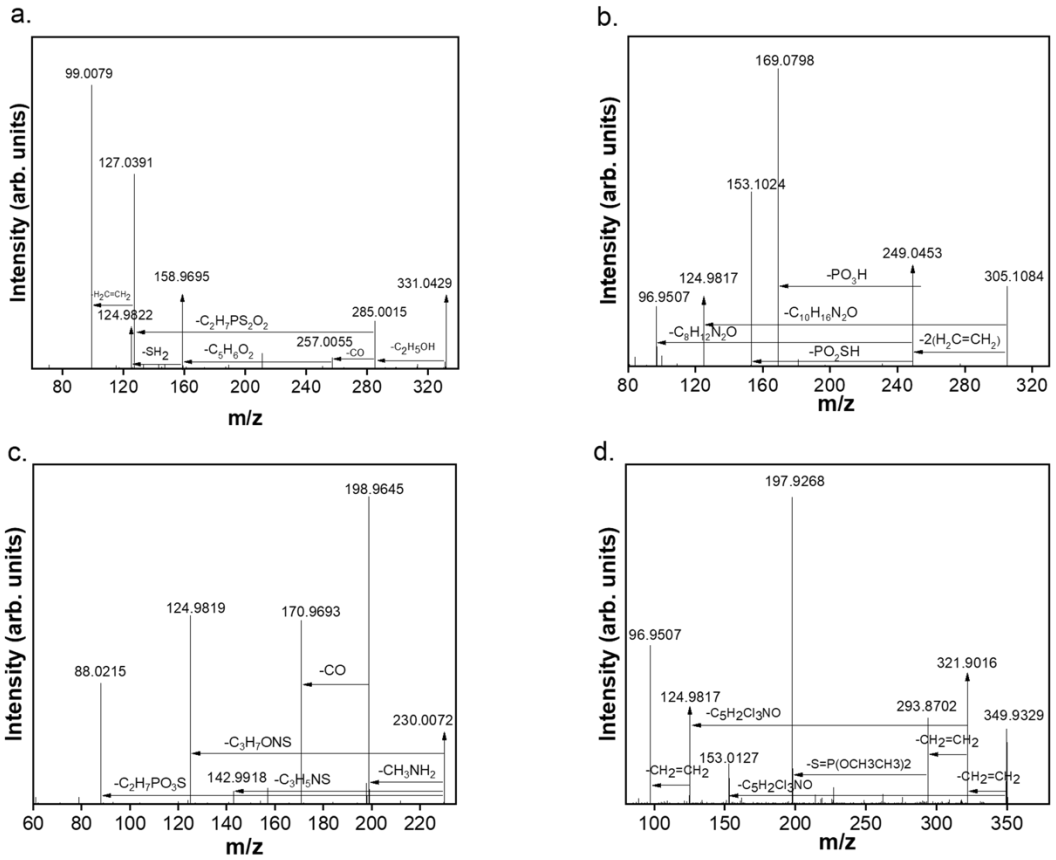

Figure 2.2: MS/MS fragmentation of a. malathion (CE = 5eV) b. diazinon (CE = 15eV) c. dimethoate (CE = 5eV) d. chlorpyrifos (CE = 10eV)

The m/z 285.0015 resulted from the loss of a 46 Da (C_2H_6O) neutral species from the precursor ion. The accurate mass (285.0015 Da) supported the elemental composition of $C_8H_{14}O_5PS_2$. Bond lengths before and after protonation were compared and the change in bond length was reported in Table 2.3. It can be seen that there is an elongation of bond 16 leading to its fragmentation to

form structure M1. This supports the experimental data where fragment 285.0011 was observed (Figure 2.5). Some previous studies[70, 83] reported that bond elongation favors fragmentation. In their study, bond elongation ≥ 0.03 Å was considered enough to result in bond cleavage. Likewise, fragment ion 257.0055 is observed in the experimental fragmentation pattern. There is a loss of $COOCH_2CH_3$ neutral species resulting in fragment 257.0055 with molecular formula $[C_7H_{14}O_4PS_2]^+$. From the computational study, elongation of bond 9 (Table 2.3) was observed which led to its cleavage leading to structure M2 (Figure 2.3).

Also, 158.9695 fragment ion was seen in the MS/MS spectrum of the experiment. Elongation of bond 7 from the DFT calculation induced its fragmentation hence resulting in a fragment ion. Loss of $C_8H_{13}O_4$ after the bond elongation led to the formation of M3 with elemental composition $[C_2H_8O_2PS_2]^+$ which was in support of the experiment. The loss of m/z 34 Da (SH_2) from fragment ion 158.9695 led to the formation of fragment ion 124.9822 with elemental composition $C_2H_6O_2PS$. From the computational study, elongation of bond 6 was observed. This led to the fragmentation of the bond hence resulting in the fragment ion 124.9822 in the experiment (structure M4 shown in Figure 2.3). In addition, the experimental data showed fragment ion 127.0391. This was obtained from the loss of $S=P(OMe)_2SH$ from fragment ion 285 $[C_8H_{14}O_5PS_2]^+$. From the DFT calculations, the elongation of bond 7 and subsequent elongation of bond 16 led to the cleavage of both bonds resulting in the fragment ion. The loss of C_2H_6O and $S=P(OMe)_2SH$ neutral species resulted in fragment ion 127.0391 as seen in the experiment. Additionally, experimental data shows fragment ion at 99.0079. A previous study indicated that the loss of $H_2C=CH_2$ from fragment ion 127.0391 resulted in this observed product ion.[72] The computational study showed the cleavage of bond 13 after bond elongation leading to the said fragment ion from M5 (Figure 2.3). Elongation of bond 11 was observed in the computational

calculation. However, this did not correspond to any of the fragment ions observed in the experiment. In addendum, the structures of the fragment ions obtained from the Metfrag analysis were in support of the DFT computational calculations (see Figure 2.4). Metfrag is a tool that combines compound database information and data from tandem mass spectrometry for the prediction of fragment ion structures.[75b]

Table 2.3: Changes in bond length (Å) of selected OPs (Diazinon[a] – original diazinon structure, Diazinon[b] – re-arranged diazinon structure)

	Malathion	Diazinon[a]	Diazinon[b]	Dimethoate	Chlorpyrifos
Bond	ΔBond length	ΔBond length	ΔBond length	ΔBond length	ΔBond length
1	-0.023	-0.013	-0.027	-0.022	0.006
2	0.006	-0.02	-0.032	0.003	-0.034
3	0.010	0.014	0.052	0.015	0.065
4	-0.015	-0.003	-0.002	-0.012	-0.003
5	0.025	-0.011	-0.027	0.006	-0.021
6	0.029	0.014	0.055	0.053	0.058
7	0.030	-0.002	-0.001	-0.016	-0.002
8	0.011	0.071	0.092	-0.017	0.099
9	0.031	-0.05	-0.008	0.070	-0.017
10	-0.020	0.023	0.020	-0.053	-0.071
11	0.074	-0.022	-0.015	0.021	0.047
12	-0.067	0.028	0.019		-0.053
13	0.038	0.023	0.018		0.040
14	-0.006	-0.028	-0.037		-0.001
15	0.008	0.016	0.003		0.066
16	0.036	-0.009	0.002		0.015
17	0.020	-0.006	0.001		-0.002
18	-0.003	0.009	0.020		-0.02
19		-0.004	0.007		

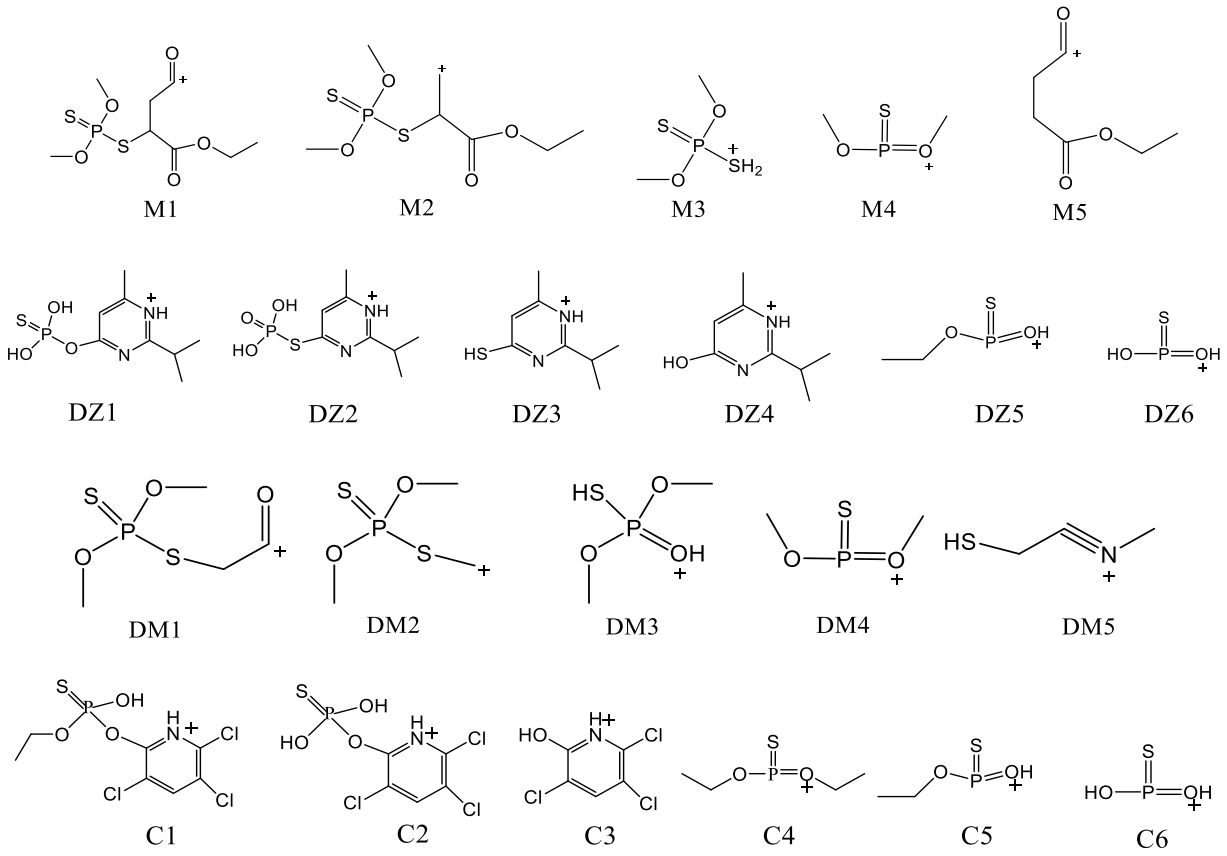

Figure 2.3: Structures of fragment ions a. Malathions' fragment structures b. Diazinons' fragment structures c. Dimethoates' fragment structures d. Chlorpyrifoss' fragment structures

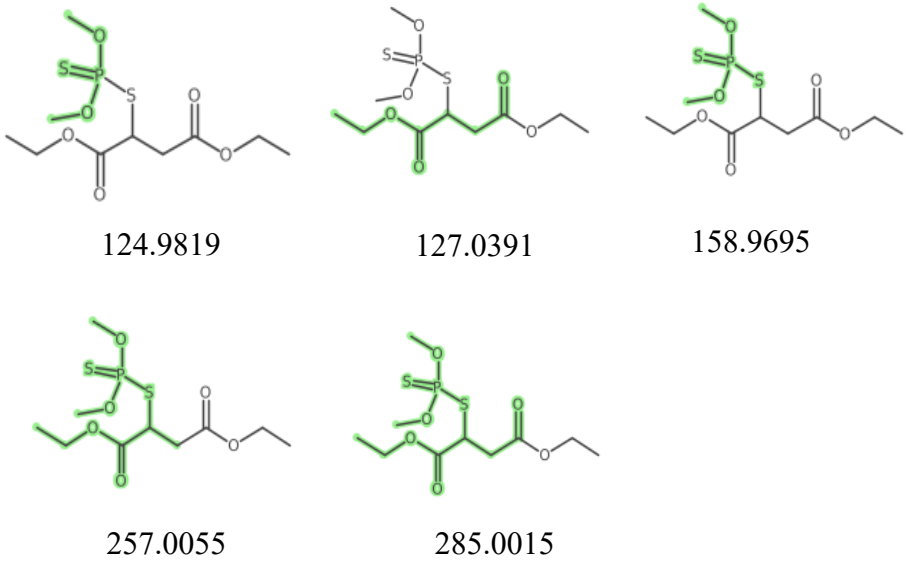

Figure 2.4: Fragment ions from structure of precursor ions obtained from using MetFrag (fragment ions are shown in green).

Note: Structures obtained from Metfrag web

2.3.3.2 Fragmentation of diazinon

Signals of product ions of protonated diazinon were found at m/z 249.0453, 169.0798, 153.1024, 124.9817, and 96.9507 (Figure 2.2 b). Similar fragment ions were observed in a previous study.[84] It was reported that there is a possible thiono-thiolo re-arrangement of diazinon structure where there is a switch between the S and O atoms (between the ring and P) atoms as shown in Figure 2.4.[84] Hence, two possible structures can be observed in the gas phase studies for the fragmentation of diazinon. For the original and re-arranged structures, an energy difference of 3.8 kcal/mol was observed with the re-arranged structure being the most stable (0.0 kcal/mol). The most stable structures after protonation revealed possible fragmentation of some bonds leading to fragment ions observed in the experiment. The signal at 249.0453 resulted from the loss of a 56-Da 2(CH_2=CH_2) neutral species from the precursor ion. The accurate mass (249.0453 Da) supported the elemental composition of $[C_8H_{14}N_2O_3PS]^+$. For this fragment ion, there is a possibility of two different structures (one from the original diazinon structure;DZ1 (Figure 2.3) and another from the re-arranged structure;DZ2). A previous study proposed structures DZ1 and DZ2 as possible fragment ions.[84] Based on DFT calculations, the relative energy of the fragment ion obtained from the re-arranged structure was 0.0 kcal/mol while that obtained from the original structure is 2.1 kcal/mol. Comparing the non-protonated structures to protonated structures, there was bond elongation of bonds 6 and 3 (Table 2.3) in the re-arranged structure to form the fragment ion observed experimentally whereas bonds 6 and 3 remained significantly the same in the original structure (bond elongation < 0.03 Å). Hence it can be said that structure DZ2 is the structure observed in the experiment. From the experimental data, accurate mass measurement 169.0798 was observed in the MS/MS spectrum of diazinon. It has been reported in a previous study that this fragment ion can only be possible when there is a thiono-thiolo re-arrangement.[84] From the

theoretical calculations in this work, after the thiono-thiolo re-arrangement (Figure 2.5), bond elongation was observed between the P and S (bond 8) leading to structure DZ3. The loss of PO_3H after the thiono-thiolo re-arrangement with subsequent loss of 2(CH_2=CH_2) led to the formation of fragment ion 169.0798 (elemental composition $[C_8H_{13}N_2S]^+$). Also, ion 153.1024 was obtained as a fragment ion in the experiment. The elemental composition $[C_8H_{13}ON_2]^+$ was deduced. This structure was formed from the cleavage of 2(CH_2=CH_2) and subsequent loss of the PO_2SH neutral species. To obtain a better insight into how the fragmentations occur, the protonated diazinon structure was compared to the non-protonated structure (original structure). From the computational calculations, elongation of bond 8 (in the original structure) led to its cleavage leading to structure DZ4. Similarly, Wright et al[83] reported possible fragments of maraviroc and its metabolite using DFT calculations. Bond elongation observed in the stable protonated structures were reported to be the primary cause of the fragmentation. Also, another study reported the bond elongation of dimethoate and omethoate resulting in bond cleavage hence resulting in various fragment ions.[70] Structure DZ4 (Figure 2. 3) was similar to the degradation product of diazinon known as 2-isopropyl-6-methyl-4-pyrimidinol (IMP). This reveals the fragmentation/degradation relationship between the fragment and the degradation product, an indication that all the other fragment ions may be possible degradation products of the parent pesticide which are not yet reported. The toxicity of these fragments is unknown hence it is important to synthesize these products and test their toxicity to ascertain their effect in order to minimize unintentional OP pesticide poisoning which may be contributed by some of these products. In addition, the results from the Metfrag analysis supported the fact that ion 169 could not be obtained from the original structure of diazinon. In the experiment, fragment 124.9817 was observed. From the theoretical calculation, elongation of bond 6 leading to the loss of CH_2=CH_2 was expected (original structure)

to support the experimental finding. However, this was not observed. The nitrogens in the pyrimidine structure were found to be the most favored protonation sites. However, a previous study reported that there are instances where fragment ions observed will be as a result of the mobile protons cleaving bonds at initially less favored protonation sites.[70, 85] It was observed that when A4 was protonated in the original structure, there was elongation of bond 6 (0.055 Å) and bond 3 (0.039 Å) leading to the cleavage of the bonds. The loss of CH_2=CH_2 after the cleavage of bond 6 and loss of $C_8H_{12}N_2O$ after the cleavage of bond 8 led to the formation of $[C_2H_5O_2PS]^+$ (structure DZ5 in Figure 2.3) elemental composition. Similarly, the loss of 2(CH_2=CH_2) after the cleavage of bond 6 and 3 and loss of $C_8H_{12}N_2O$ after the cleavage of bond 8 led to the formation of $[H_2O_2PS]^+$ (structure DZ6) elemental composition. The discussed fragment ions (together with their respective structures) may be possible degradation products of diazinon that can be further investigated for their toxicological effects.

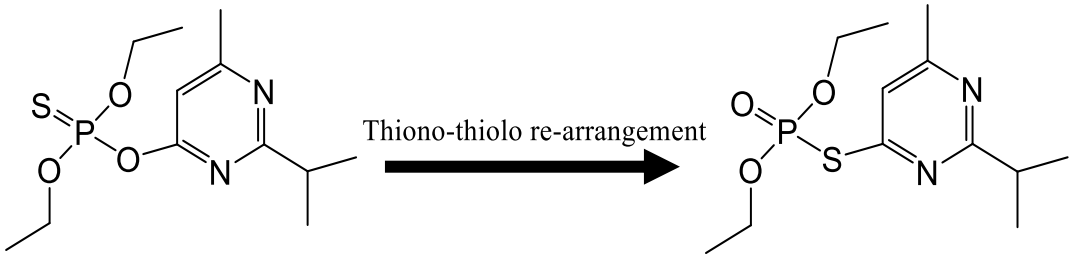

Figure 2.5: Thiono-thiolo re-arrangement of diazinon structure, original structure (left), structure after re- arrangement (right)

2.3.3.3 Fragmentation of dimethoate

Major product ions of protonated dimethoate were found at m/z 198.96406, 170.96931, 142.99184, 124.98460, and 88.0215. Fragment ions are briefly discussed below. The experimental MS/MS fragmentation spectrum is shown in Figure 2.2c. The product ion 198.9645 was derived from the loss of 31 Da neutral species from the precursor ion 230.0072. Accurate mass measurement

revealed that m/z 198.9645 corresponds to the elemental composition $[C_4H_8O_3PS_2]^+$ and thus proved the absence of the N atom. Therefore, the fragment ion at m/z 198.9641 was assigned to structure DM1 (Figure 2.3) produced by the loss of methylamine, CH_3NH_2 (31 Da).[70] Even though the carbonyl oxygen is reported as the most stable site of protonation, it is reported that protons are mobile and have the ability to cause cleavage of bonds at initially less favored protonation sites.[70, 85] From the DFT calculations there was contraction of bond 10 when the most likely protonation site (stable) was considered. However, there was elongation of bond 10 when the amide-N atom was protonated, which revealed the cleavage of methylamine leading to the formation of a stable acylium ion[86] consistent with the findings of John and co-workers.[70]

The loss of a 59-Da neutral species from the parent ion m/z 230.0072 resulted in the signal 170.9693. The accurate mass 170.96931 Da supported the elemental composition of $[C_3H_8O_2PS_2]^+$. In accordance with other reports, [70, 87] it is therefore concluded that loss of CH_3NHCHO resulted in the fragment ion 170.9693. Based on the DFT calculations, it was found that bond 8 shortened. Hence it can be assumed that structure DM2 was obtained through a consecutive process during the elongation of bond 9 and 10.[70] 142.9918 Da accurate mass measurement was observed in the experiment. This led to the conclusion of molecular formula $C_2H_8O_3PS$ which is in accordance with the fragment ion reported elsewhere.[70, 87] Therefore, $[HSP(OMe)_2OH]^+$ was the proposed structure. From DFT calculations, none of the protonations leading to the various bond elongations could be attributed to m/z 142.9918. Hence it can be concluded that this could be as a result of consecutive reactions instead of a single bond cleavage as proposed by John and his co-workers.[70] Also, the loss of 105 Da neutral species led to fragment ion 124.9811 in the experiment. The elemental composition $[C_2H_6O_2PS]^+$ deduced confirmed the absence of N which corresponds to the relatively odd mass number. From the DFT calculations,

there was elongation of bond 6, an evidence supporting its cleavage leading to structure DM4. Masses with odd numbers suggest even number of N atoms or the absence of N atom in the molecular formula.[88] Elongation of bond 6 resulting in its cleavage led to fragment ion 124.9811. The subsequent elongation of bond 6 and 9 in the precursor ion, led to the formation of fragment 88.0215 with elemental composition $[CH_3NCCH_2SH]^+$ (structure DM5).

2.3.3.4 Fragmentation of chlorpyrifos

Signals of major product ions of protonated diazinon were found at m/z 96.9507, 124.9817, 153.0127, 197.9268, 293.8702, and 321.9016 (Figure 2.2d).

Accurate mass measurement 321.9016 Da resulted from the loss of a 28-Da (CH_2=CH_2) neutral species from the precursor ion 349.9329. The accurate mass (321.9016 Da) supported the elemental composition of $[C_7H_8Cl_3NO_3PS]^+$. Based on the DFT calculations, there was elongation of bond 3 after protonation in the most stable structure (Table 2.3). This led to the cleavage of this bond resulting in structure C1 (Figure 2. 3) as observed in the experiment. Additionally, fragment ion 293.8702 resulted from the subsequent loss of 28-Da (CH_2=CH_2) neutral species from fragment ion 321.9016. The accurate mass (293.8702 Da) supported the elemental composition of $[C_5H_4Cl_3NO_3PS]^+$. Based on the computational calculations, elongation of bond 6 was observed leading to the cleavage of this bond. This resulted in the structure C2 (Figure 2. 3) as observed in the experiment. There was loss of 152-Da to form the fragment ion 197.9268. This resulted from the loss of $C_4H_9O_2PS$ neutral species from the precursor ion and matches the fragmentation pattern reported previously.[89] The accurate mass (197.9268Da) supported the elemental composition of $[C_5H_3Cl_3NO]^+$. In comparison of the most stable protonated structure to the non-protonated structure, there was elongation of bond 8 which led to its cleavage leading to the formation of

structure C3 (Figure 2. 3). This supports the experimental results. Structure C3 is similar to one of the degradation products of chlorpyrifos known as 3,5,6-trichloro-2-pyridinol (TCP). Here also, the fragmentation/degradation relationship between the fragment and the degradation product of chlorpyrifos is revealed. Also, the loss of $C_5H_2Cl_3NO$ after the cleavage of bond 8 in the DFT calculations resulted in structure C4 supporting the elemental composition $[C_4H_{10}O_2PS]^+$. This is in agreement with the elemental composition proposed by Yunhee and co-workers.[90] Furthermore, the cleavage of bond 8 (loss of $C_5H_2Cl_3NO$) and bond 6 (loss of $CH_2{=}CH_2$), from the precursor ion resulted in structure C5 with the elemental composition $[C_2H_6O_2PS]^+$. From the accurate mass measurement of the MS/MS experiment of chlorpyrifos, fragment ion 96.9507 was observed. Subsequent fragmentations of bond 3, 6 and 8 after bond elongations led to structure C6 which supported the elemental composition $[H_2O_2PS]^+$. Elongation of bond 11, 13 and 15 was observed in the theoretical calculation. However, these elongations do not correspond to any of the observed fragment ions. Sinha et al. reported a possible fragment of chlorpyrifos with elemental composition $[C_4H_2NOCl_2]^+$.[89b] The proposed structure in their study corresponds to m/z ~150 which was not observed in the current study. The possibility of this fragment may explain the elongation of bonds 11, 13 and 15 as there is loss of CCl from structure C3 and re-arrangement to form the structure proposed in the previous study.[89b]

2.3.3.5 Trend in the Organophosphate Fragmentation

The trend in the fragmentation of the two types of organophosphates used in this study was investigated. For all the four organophosphates (two different types) studied, a similar fragment ion (124.98) was observed. This is consistent with a report from a study which revealed that the fragment ion (124.98) is a diagnostic ion for organophosphates.[91] However, the cleavages leading to the fragmentations observed using the computational study were not the same for the two types

of OPs investigated. Malathion and dimethoate have two methoxy groups attached to the phosporus atom and S=P–S bond (type 1) whereas chlorpyrifos and diazinon have two ethoxy groups attached to the phosporus atom and S=P–O bond (type 2). There was similarity in the cleavage of the bond that resulted in ion 124.98 for malathion and dimethoate as well as similar cleavage observed for chlorpyrifos and diazinon. For the organophosphates with two methyl groups attached to the two oxygen atoms, there was cleavage of the P–S bond which resulted in the fragment ion. In contrast, there was cleavage of P–O bond and subsequent loss of CH_2=CH_2 of the organophosphates with two ethyl groups attached to the oxygen atoms, which resulted in the aforementioned fragment ion. This observed pattern is also confirmed by the Metfrag analysis. For the type 2 organophosphates, a similar fragment ion at 96.95 was observed whereas this fragment ion was not observed for the type 1 organophosphates. This may be due to the presence of the two ethoxy groups attached to the phosporus atom (in the type 2 organophosphates) which yields to fragmentation of two ethylene groups (more stable)[92] whereas no fragmentation is observed in the methoxy groups attached to the phosporus atom (type 1) as the resulting methylene group after fragmentation would be less stable. This is confirmed in the computational study where there is elongations of bonds 3 and 6 for the type 2 OPs where no elongation of bond 3 and 5 in the type 1 OPs was observed.

2.4 Conclusion

Fragmentation pattern of organophosphate pesticides are reported using both experimental and theoretical approaches. Elongation of bond lengths after protonation mostly led to bond cleavage resulting in a fragment ion. DFT computation produced relevant data to identify product ions of malathion, dimethoate, chlorpyrifos and diazinon supporting experimental MS/MS fragmentation of the organophosphate pesticides. In spite of the same fragment ion observed for the two types of

OPs investigated in this work, the computational study revealed a difference in their fragmentation pathway. This indicates that, even though all the OPs in this study showed similar fragment ion (124.98), their fragmentation pathway was used to differentiate between the two types of OPs.

Also, based on fragmentation/degradation relationship, the various fragment ions observed in the experiment and supported with the computational findings were predicted as possible degradation products of the OP pesticides investigated. These structures (the possible degradation products) can be synthesized, and their toxicity level tested in order to decrease unintentional pesticide poisoning by OPs as they may be a contributing factor to the numerous cases.

3.0 **Screening of pesticides using Liquid chromatography ion mobility mass spectrometry (LC-IM-MS) and Paper Spray Ion Mobility Mass Spectrometry (PS-IM-MS)**

3.1 Introduction

Pesticides are very important in crop production as they have increased crop yields significantly yet they can affect human health and contaminate natural resources.[93] Organophosphates (OPs) and triazines[94] are commonly used pesticides in agriculture. OPs are insecticides with the majority being highly toxic.[63-64] They are extensively used over the world in crop production[64] due to their low cost, low persistent nature in the environment, and the ability to eliminate many pests[63]. A study reported that acute or chronic exposure to organophosphorus compounds, such as OPs, can cause neurotoxic disorders.[66b] Organophosphates pesticides may cause detrimental effects in humans[66b, 95] such as inducing malignant transformation of breast cells.[66b, 95-96] OPs act by inhibiting the enzyme acetylcholinesterase in the central nervous system (CNS) of humans and insects, which leads to its malfunction.[97] Diazinon and chlorpyrifos are among the list of most commonly used OPs registered by the Environmental Protection Agency (EPA) of the United States[67] and are reported to be hazardous.[98] A recent study showed that exposure to diazinon[68] could be a possible cause of breast cancer in females. Natural killer (NK) cells play a vital role in the immune defense against human viral infections and tumor development.[94a, 99] Therefore, any agent that interferes with the function of NK cells to perform their function could increase the incidence of tumor and/or the risk of viral infections. Triazines are reported to decrease the cytotoxic function of the human NK cells.[100] For the many reasons above, fruits and vegetables are screened by regulatory authorities prior to their entry into markets. The regulation is aimed at ensuring fruits and vegetables do not enter the markets with intolerable pesticide content.[101]

Most often, the screening of fruits and vegetables are conducted in search for parent pesticides with neglect of their degradation products.[102] It is, however, established that some pesticides degrade to form more toxic and persistent compounds than their parent pesticides.[70, 72, 82]

For instance, it has been reported that dimethoate undergoes desulfuration to produce more toxic omethoate, which can induce cholinergic crisis and eventually lead to death.[70] Similarly, diazinon undergoes oxidative desulfuration to form diazoxon and hydrolysis to form 2-isopropyl-6-methyl-4-pyrimidinol.[103] The degradation products of diazinon are reported to be more potent acetylcholinesterase inhibitor[104] and have stronger genotoxic potential[105] than the parent compound. For consumption purposes, it is necessary to include degradation products of toxicological concerns in analysis. This issue may be of significance if the parent pesticide has degraded, but the degradation products are still detectable.

Analysis of pesticides and their degradation products is usually performed by tandem GC-MS or LC-MS/MS, using different analyzers such as single quadrupole, triple quadrupole analyzers (QqQs), ion trap (IT), quadrupole time of flight (QTOF) or time of flight (TOF).[72, 82a, 106] Nevertheless, the physicochemical properties of pesticides and their degradation products (typically higher polarity and solubility) make LC-MS/MS the most suitable technique for their determination.[72] In spite of the success with LC-MS/MS, there is difficulty in using this technique to differentiate between some isomeric pesticides which are currently in use.[6] In the LC-MS/MS technique, pesticide precursor ions are selected for fragmentation and identification. Hence, degradation products would be missed in instances where the parent pesticides are degraded.

Based on the foregoing discussion, there is a need for new, and efficient analytical techniques for identification of pesticides and their degradation products in complex samples. Thus, if the

degradation products of pesticides are known, it becomes easier to map out to the parent pesticide for robust analysis. This would reduce false negative and/or false positive results.

In this work, liquid chromatography ion mobility mass spectrometry (LC-IM-MS) was proposed as a remedy for the efficient identification of pesticides and their degradation products. LC-IM-MS offers an enhanced approach for the identification of pesticides and their degradation products. It benefits from additional descriptors collectively used to determine the CCS values in addition to retaining m/z and retention times for easy compound identification. Note that in an event of compound degradation, IM has a unique and additional capability of determining the CCS values of degraded compounds for their easy identification. Also, collision induced dissociation can be performed on the parent pesticides and degradation product as well. These complementary features of LC-IM-MS give it a competitive edge over the conventional LC-MS/MS approach.

On the other hand, ambient ionization techniques have been utilized to ionize samples directly in their native environments. Ambient ionization methods are new approaches pertinent to the direct analysis of samples in their ambient states, followed by mass spectrometric analysis[26]. As described earlier,[33] paper spray is an ambient ionization technique in which a solid or liquid sample is preloaded to the surface of paper substrate. The sample spotted onto the paper is allowed to dry and positioned 5-10 mm away from the inlet of the mass spectrometer. Spray solvent is applied to the paper where it interacts with the sample and extracts any soluble components. The application of solvent transports the analytes in the complex matrix or sample to the tip of a triangle paper under the influence of high voltage (usually in 3-5 kV range)[34]. Upon arrival to the tip of the paper positioned in front of the mass spectrometer inlet, electrospray occurs, and the resulting ions are detected by mass spectrometry[33-34].

Paper spray mass spectrometry (PS-MS) has been used successfully for the screening of pesticides

in food matrices.[57] However, none of these studies involved isomeric pesticides. This may be due to difficulty in differentiating between isomeric pesticides due to the same m/z. Isomers with different structural shape and size can be differentiated using IM technique. When this technique is incorporated into paper PS-MS, it would make pesticide screening using this approach more effective. PS-IM-MS offers an enhanced approach to the identification of compounds. It benefits from additional CCS values to m/z for easy analyte identification. In the LC-IM-MS method, a total of 13 minutes was used in the separation and identification of analytes whereas 1 min was utilized in PS-IM-MS. The rapid analysis time in combination to the use of CCS values and m/z in PS-IM-MS for analyte identification gives it a competitive edge to LC-MS/MS. PS-IM-MS has been used successfully for the separation of isomeric compounds in a previous study.[59] CCS measurements results in reliable identification of isomeric and non-isomeric parent pesticides as well as their degradation products. Recent studies revealed that CCS values of structures could be predicted through computational calculations.[107] To this end, computational calculations were performed to determine CCS values of the considered pesticides to complement the experimental data.

In the current study, four parent pesticides (propazine, terbuthylazine chlorpyrifos, diazinon) and their degradation products; 2-isopropyl-6-methyl-4-pyrimidinol (IMP), atrazine-desethyl (DEA), atrazine-desisopropyl (DIA), and 3,5,6-trichloro-2-pyridinol (TCP) are investigated using LC-IM-MS and a rapid PS-IM-MS method. Also, a pesticide mixture is prepared and spiked into spinach extract for screening and identification. In addendum, density functional theory (DFT) structure calculations provide synergistic insights for the identification of parent pesticides and their degradation products. DFT allows for the approximation of kinetic parameters with a sufficient degree of accuracy and at a significant computational cost.[108] For this study, non-protonated

structures were initially optimized using a DFT functional. Natural bond orbital (NBO) analysis[109] was used for selecting potential protonation sites and theoretical CCS values calculated using IMoS software. [107b, f] Theoretical and experimental CCS values are compared for identification of the structures of the parent pesticides and degradation products. This work therefore presents a systematic study on the identification of the parent pesticides and their degradation products.

3.2 Experimental Methods

3.2.1 Chemicals and sample preparations

Chlorpyrifos, propazine, terbuthylazine, diazinon, atrazine-desethyl, atrazine-desisopropyl, and 3,5,6-trichloro-2-pyridinol standards were purchased from Sigma-Aldrich. 2-isopropyl-6-methyl-4-pyrimidinol was purchased from Chem Service Inc. High purity solvents: formic acid, ACN, and ultra-pure water were purchased from Agilent Technologies (Santa Clara, CA), and were used throughout the duration of the experiment. Syringe (captiva disposable Syringe, 10 mL, polypropylene, p/n: 9301-6474) and syringe filters (captiva econofilter, nylon membrane, 13 mm diameter, 0.2 µm pore size), p/n: 5190-5269, Agilent SampliQ QuEChERS AOAC Extraction kits (p/n 5982-5755) and QuEChERS Dispersive Kit, Universal, AOAC method (p/n 5982-0029) were obtained from Agilent Technologies Inc., DE, USA. ESI tuning mix (low concentration) was purchased from Agilent Technologies (Santa Clara, CA). All chemicals and reagents were used without further purification. 1 mg/mL (1000 ppm) stock solution were prepared in ACN (ACN). The stock solutions were diluted to 10 ppb using 75 % ACN except for chlorpyrifos and TCP where 100% ultrapure water was used for the dilution.

Table 3.1: Parent pesticides and degradation products, classes, and chemical structures.

Pesticides	**Class**	**Structure**	**m/z**
Terbuthylazine	Triazine	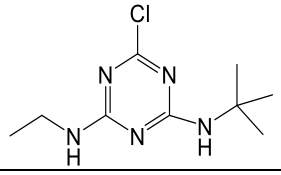	230.1172
Propazine	Triazine	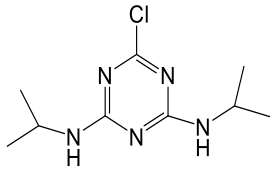	230.1172
Diazinon	Organophosphate	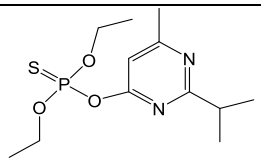	305.1083
Chlorpyrifos	Organophosphate	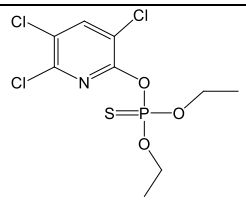	349.9336
Degradation products	**Corresponding parent pesticides**		
Atrazine-desisopropyl	Terbuthylazine	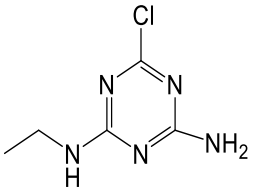	174.0541
Atrazine-desethyl	Propazine	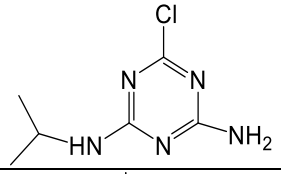	188.0696
2-isopropyl-6-methyl-4-pyrimidinol	Diazinon	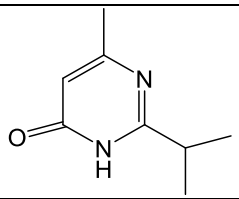	153.1022
3,5,6-trichloro-2-pyridinol	Chlorpyrifos	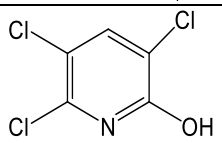	195.9129

3.2.3 Instrumentation

The HPLC utilized was Agilent 1290 Infinity II which comprises of a binary pump, multi-sampler and a heated column compartment. LC separations were performed using Agilent Infinity Poroshell 120 EC-C18, 2.1 x 50 mm, 1.9 µm (p/n 699675-902), column temperature 45 ^{o}C at a flow rate of 0.4 ml/min, and a pressure limit of 1200.00 bar. 10 µl sample was injected and analyzed. An isocratic method of H_2O - ACN (98:2, v/v) was used from time t=0 min to t=1 min, then a H_2O - ACN gradient (71:29, v/v) at time t=2.5 min, (66:34, v/v) at time t=4 min, (10:90, v/v) at time t=10.5 min, and (2:98, v/v) at time t=11 min was used with a post run time of 2 min. Mobile Phase A comprised of 0.1 % formic acid in H_2O and mobile phase B was ultrapure ACN. Needle wash: 1:1:2 H2O/ isopropyl alcohol (IPA)/MeOH. All experiments were performed using Ultra high performance liquid chromatography (UHPLC) coupled to a commercial drift tube ion mobility mass spectrometry (Agilent Technologies, Santa Clara, CA).[20a, 21b, 110] A brief description is provided here; the major components include an electrospray ion (ESI) source, a high-pressure front ion funnel, a trapping ion funnel, a uniform field drift tube, a rear ion funnel, a quadrupole mass filter, a collision cell, and a high-resolution time-of-flight mass analyzer. After the ions are generated in the ion source region, they are transferred to the high-pressure front funnel through the single-bore glass capillary. The gas phase ions are efficiently collimated and transferred into the trapping funnel (hourglass-shaped) while excess gas and neutral molecules are removed. Short discrete packets are pulsed (150 µs) into the drift tube using the trapping ion funnel. An applied weak electric field (18.5 V/cm) in the drift tube accelerates the ions while they are decelerated as they collide with the nitrogen buffer gas molecules (maintained at 3.95 Torr) resulting in analyte separation by IM.[111] Preceding to mass analysis, the rear funnel refocuses ions exiting the drift tube into the quadrupole mass filter. In order to obtain fragmentation pattern, the quadrupole mass

filter isolates the ions into the collision cell where collision induced dissociation (CID) is performed at different collision energies. Mass spectra (positive mode) were obtained over the range of m/z 100 – 1700 in profile mode where the TOF was operated in high sensitivity mode with a resolution of ~25,000. All spectra were acquired using Mass Hunter Acquisition Software B.09.00 (Agilent Technologies, Santa Clara, CA). Acquired data were visualized primarily using IM-MS Browser B.10.0 and Mass Hunter Qualitative Analysis 10.0Ink and exported to Microsoft Excel for additional in-depth analyses. Graphs and plots were generated using Origin version 2018b (64-bit) b9.5.5.409 (Academic). All experiments were performed in the positive mode. The IM-MS settings used herein are as follows; 325 ^{o}C gas temperature at a flow of 5 l/min, 35 psi nebulizer, 275 ^{o}C sheath gas temperature at a flow of 11 l/min, 3500 V capillary voltage, 1000 V nozzle voltage, 400 V fragmentor voltage, 0.9 frames/s; 18 IM transients/frame; 60 ms maximum drift time; 600 TOF transients/IM transients; 20,000 µs trap fill time; and 250 V drift tube exit voltage. For the purpose of daily instrument mass calibration, Agilent tune mix solution was used.

3.2.4 Paper Spray Ion Mobility Mass Spectrometry (PS-IM-MS)

A Whatman grade 1 filter paper was cut into a triangle (10 mm high and 8 mm base width) and used. A copper clip mounted onto a 3-dimensional moving stage was used to hold the paper triangle with the tip of the paper held in line with the instrument inlet. 3 µL of the pesticide sample was spotted directly onto the center of the paper triangle using a micropipette and allowed to air dry. A zero voltage was applied to the paper via the copper clip connected to the grounded outlet of the mass spectrometer, and the capillary voltage was set to +3.5 kV and -3.5 V for negative and positive mode respectively as in a previous study.[59] 5 µl of MeOH was applied to the paper at once using a micropipette, and a new strip of paper was used for each analysis.

All experiments were performed using a commercial drift tube ion mobility mass spectrometry (Agilent Technologies, Santa Clara, CA).

3.2.5 Computational Details

Density functional theory (DFT) calculations were carried out using the Gaussian 16[76] software package. Geometry optimization and vibrational frequency analysis and NBO analysis were performed using hybrid density functional B3LYP method in combination with 6-31G(d,p)[109] basis set. A zero-point energy correction was performed for all calculated structures. Basic sites of the pesticides were selected based on NBO analysis, protonated individually and the optimized geometry of each ionic species determined. The relatively stable structures for the parent pesticides and degradation products were also optimized at MP2/6-31G++(d,p) level of theory for comparison.[112] Also, for better insight on how fragmentation of the analytes occur, bond lengths of stable protonated structures were compared to the corresponding non-protonated structures. CYLview was used for visualization and illustration of all the optimized structures.[113]

3.2.6 Theoretical CCS Calculations

Stable optimized structures obtained from gaussian output files were converted to IMoS input file using the Speed application (part of IMoS package). The CCS of the structures were calculated using IMoS software v1.10.[107b, f] using trajectory (TJ) method, at 3.95 torr and 300 K.[107f]

3.2.7 Spinach sample preparation with QuEChERS

The AOAC QuEChERS method was utilized in the sample preparation step (Figure 3.1).[114] Firstly, two ceramic homogenizers were added and organic spinach sample was homogenized.

Then, 15g of the homogenized sample was weighed into a 50 ml centrifuge tube. 15 ml of ACN (1% acetic acid) was added and vortexed (1 min). Pre-weighed salt was added and shaken (1 min) then centrifuged for 5 minutes at 4000 rpm. 8 ml of the supernatant liquid was transferred into an Solid phase extraction (SPE) tube. Sample was vortexed for 1 min and centrifuged at 4000 rpm for 5 minutes. The extract was transferred into a syringe and filtered through a 0.2 µm nylon membrane (Captiva Econofilter, nylon membrane, 13 mm diameter, 0.2 µm pore size). 1:4 dilution was made after filtration, and sample analyzed. Samples were pre- and post-spiked with pesticide mixture.

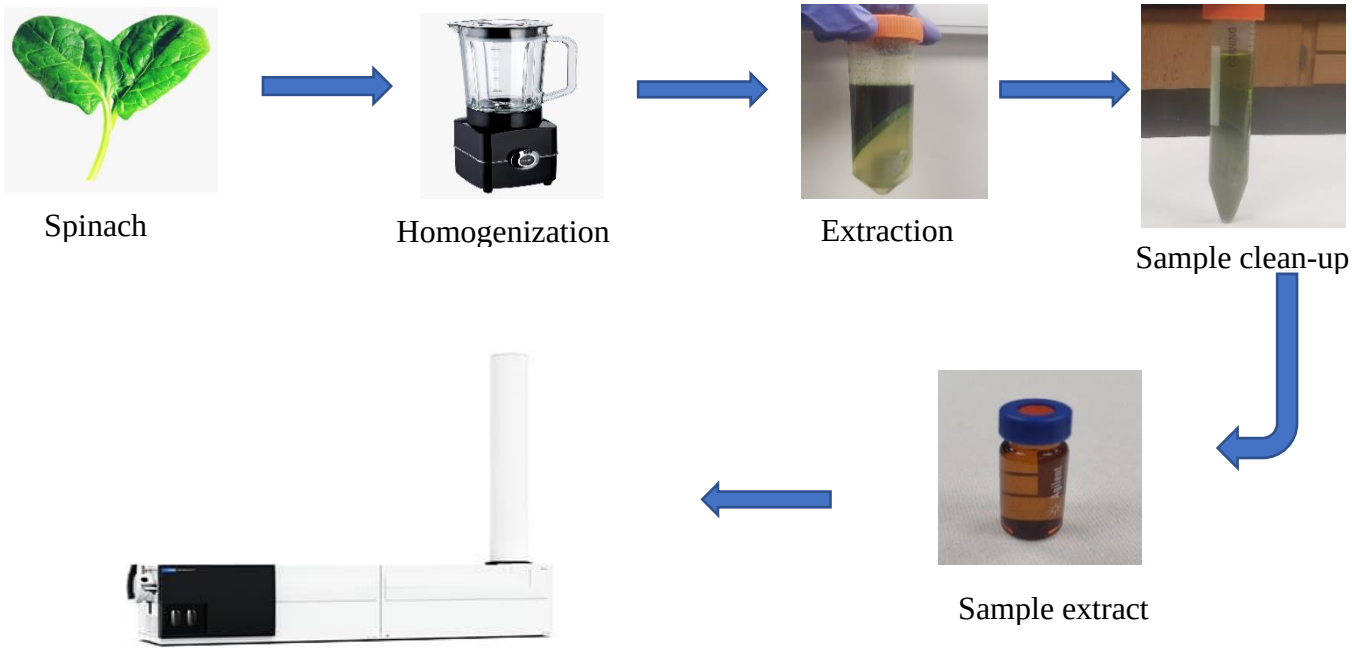

Figure 3.1: Steps in QuEChERS sample preparation for spinach.

3.2.8 Post data acquisition

For data files collected using multiplexed acquisitions, PNNL PreProcessor was used for initial interpolating, smoothing and demultiplexing[115] to reconstruct the signal. An increased sampling density was needed to support higher drift resolution which was achieved using drift bin

interpolation of 3. Ion mobility feature extraction (IMFE) algorithm in the MassHunter IM-Browser, it was used to extract the targeted list and exported. Data was then processed using the high resolution demultiplexer (HRdm).[4c] The default value was utilized for m/z width multiplier and the high-resolution processing level was fixed at high.[4c] The instrument function multiplier was set at 1.00 for the 4-bit multiplexed acquisition. The feature list, raw multiplexed data and the reconstructed demultiplexed data after PNNL processing were used by the software to deconvolute the peaks.[4c] Data files acquired using single pulse acquisitions were processed using the MassHunter IM-Browser.

3.2.9 Atomic charges and protonation site selection

NBO analysis is a tool that facilitates the interpretation of electronic structure calculations in a chemically intuitive manner.[77] Figure 3.2a-d displays the numbering of the more negative atoms in diazinon, chlorpyrifos, propazine and terbuthylazine while Table 3.2 displays their NBO atomic charges at B3LYP/6-31G(d,p) level of theory. Same analogy was applied for the degradation products. The possible protonation sites were selected based on the NBO analysis. The structure with the lowest energy was selected as the most stable structure. Bock et al[78] selected protonation sites of both N-(6-methoxypyridin-3-yl)-4-(pyridin-2-yl)thiazol-2-amine mono-hydrobromide monohydrate and N-(6-methoxypyridin-3-yl)-4-(pyrazin-2-yl)thiazol-2-amine mono-hydrobromide based on the difference in electron density provided after NBO calculations. The atoms with the negative natural atomic charge were selected for the protonation sites of the cations where the protonation sites were selected based on NBO analysis by using the more negative atoms.[79] Herein, NBO was chosen for the atomic charge distribution calculation. From the results, the labelled atoms in Figure 3.2 were selected for protonation due to their possession of more negative atomic charges hence are likely protonation sites ($\geq$ -0.5).[78-79]

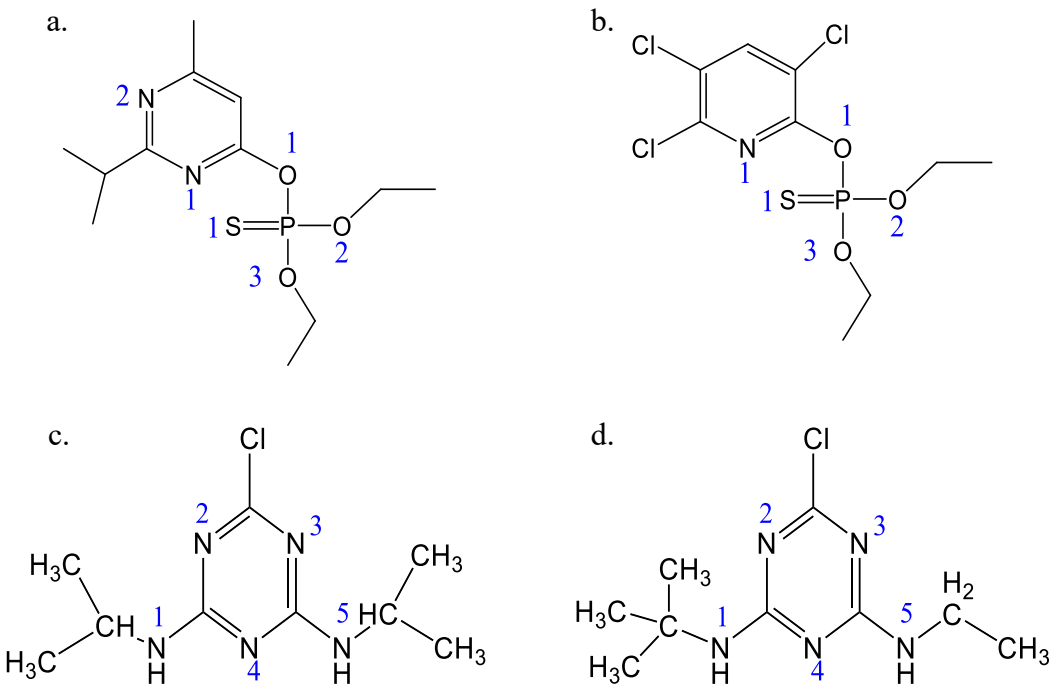

Figure 3.2: Structure of parent pesticides for possible protonation site selection. a. diazinon b. chlorpyrifos c. propazine d. terbuthylazine

Table 3.2: NBO charge distribution of parent pesticides (diazinon, chlorpyrifos, propazine and terbuthylazine

Diazinon		**Chlorpyrifos**		**Propazine**		**Terbuthylazine**	
Atom	**NBO**	**Atom**	**NBO**	**Atom**	**NBO**	**Atom**	**NBO**
N1	-0.546	N1	-0.484	N1	-0.621	N1	-0.624
N2	-0.517	O1	-0.777	N2	-0.587	N2	-0.587
O1	-0.787	O2	-0.843	N3	-0.604	N3	-0.608
O2	-0.845	O3	-0.859	N4	-0.622	N4	-0.626
O3	-0.858	S1	-0.571	N5	-0.619	N5	-0.618
S1	-0.584						

3.3 Results and Discussion

3.3.1 Screening of pesticides using LC-IM-MS

3.3.1.1 Mobile phase selection

Two different mobile phases (ACN and methanol) on the LC separation of 14 pesticides in a pesticide mixture were examined as shown in Figure 3.3. It was observed that there was co-elution of two of the analytes when MeOH was used as the mobile phase. There was less co-elution of the

analytes when ACN was used. Hence, ACN (100%) was chosen due to its high separation of the 14 pesticides in a commercial pesticide mix (Agilent Technologies).

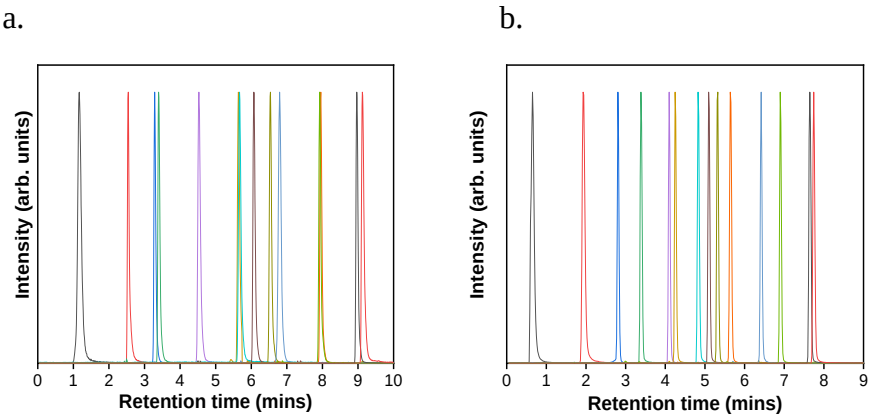

Figure 3.3: LC-Separation of pesticides using different mobile phases a. methanol b. acetonitrile

3.3.1.2 LC-IM-MS separation of mixture of parent pesticide and degradation products

A pesticide mixture was prepared using four parent pesticides and their degradation products in this work (see Table 3.1). The mixture was analyzed using LC-IM-MS and the corresponding CCS values of each pesticide reported in Table 3.3. Most often, the screening of fruits and vegetables is conducted in search for parent pesticides with neglect of their degradation products.[102] It is an established fact that some pesticides degrade to form more toxic and persistent compounds than their parent pesticides.[70, 72, 82] Diazoxon and IMP are two of the major degradation products of diazinon.[84, 116] It is reported that diazinon and these two degradation products had toxic effects on the brain synaptosomes of rats.[82b] The most toxic compound among the parent pesticide and the two degradation products was found to be diazoxon. It is known that IMP is a non-toxic metabolite of diazinon.[82b, 117] However, a study showed that it induced superoxide dismutase stimulation up to 30% implicating it to be a plausible toxic metabolite.[82b]

Table 3.3: Retention time (RT), m/z and experimental CCS of parent pesticides and their degradation products.

Num.	Pesticide	RT	m/z	Exp. CCS
1	2-isopropyl-6-methyl-4-pyrimidinol (IMP)	2.1 ± 0.1	153.1022	132.3 ± 0.5
8	Diazinon	7.9 ± 0.1	305.1083	172.8 ± 0.5
2	3,5,6-trichloro-2-pyridinol (TCP)	4.9 ± 0.1	197.9275	132.0 ± 0.5
7	Chlorpyrifos	9.2 ± 0.1	349.9336	165.6 ± 0.4
3	Atrazine-desisopropyl (DIA)	2.6 ± 0.1	174.0541	134.2 ± 0.3
5	Terbuthylazine	6.0 ± 0.1	230.1172	153.8 ± 0.3
4	Atrazine-desethyl (DEA)	3.0 ± 0.1	188.0696	139.8 ± 0.3
6	Propazine	5.8 ± 0.1	230.1172	155.1 ± 0.3

Diazinon and IMP had different structural shape and size as well as m/z. It was observed that the degradation products eluted before the parent pesticides in the LC (Table 3.3). Accurate mass measurements of 305.1083 and 153.1030 were utilized for the identification of diazinon and IMP in the MS (Figure 3.4). Due to difference in the structural shape and size of both parent pesticide and degradation product, they interacted differently with the buffer gas in the drift tube resulting in different arrival times leading to distinctive CCS values. CCS values of 132.3 ± 0.5 $Å^2$ and 172.8 ± 0.5 $Å^2$ was obtained for IMP and diazinon respectively. CCS value of 173.15 $Å^2$ is reported for diazinon elsewhere[118] which is similar to the obtained value with a difference of 0.2%.

Due to differences in polarity of terbuthylazine and DIA, they were separated in the LC. There was further separation in the IM which resulted in different arrival times hence resulting in different CCS values of analytes. Accurate mass measurement of 230.1177 and CCS value of 153.8 ± 0.3 $Å^2$ were used to identify terbuthylazine. A single peak was observed for DIA when separated in the LC at a retention time of 2.6 minutes indicating a single analyte. However, similar to DEA, a peak with shoulder was observed in the drift spectra of DIA (Figure 3.5c). CCS value of the peak with the highest intensity was 134.2 ± 0.3 $Å^2$. Results from the computational study revealed three relatively stable protomers with relative energies of 0.0 kcal/mol, 0.4 kcal/mol and 4.9 kcal/mol corresponding to CCS values of 138.92 $Å^2$, 139.32 $Å^2$ and 139.36 $Å^2$ showing percent difference

of 0.3% and 0.03%. Since the difference in CCS of the protomers are ≤1%, the observed shoulders cannot be attributed to the protomers obtained theoretically.

Propazine and atrazine-desethyl in the pesticide mixture were separated in the LC with retention times 5.8 minute and 3.0 minute (Table 3.3). The accurate mass measurements were used in the identification of both analytes; 230.1177 for propazine and 188.0696 for DEA. Both were also separated in the drift tube as they had different interaction with the buffer gas due to differences in their structural shape and size. Different arrival times were obtained for both analytes and their corresponding CCS values determined. Figure 3.4 shows the multi-dimensional separation of the pesticide mixture. In this study, the CCS value of propazine was 155.1 ± 0.3 $\dot{A}^2$. A previous study reported the CCS of propazine to be 155.54 $\dot{A}^2$ which is ~0.3% difference in %CCS compared with the obtained result.[119] A single peak was observed in the LC for DEA (Figure 3.5b). However, a peak with a shoulder was observed in the IM spectrum (Figure 3.5d). This was not surprising as a recent study reported that they observed double peak for paracetamol in the IM spectrum.[120] They indicated the peaks to be conformers of paracetamol and attributed either structural flexibility or difference in protonation sites of the analyte to be the reason. Paracetamol has similar structural shape and size as DEA.[120] The computational study revealed two protomers for DEA with 0.4 kcal/mol difference in energy. Also, a 0.2% difference in CCS was observed for the protomers (see Figure A3) indicating that the shoulder observed in the IM peak are not protomers. Dodds and co-workers reported that DTIMS of ~60 resolution cannot resolve peaks with less than 1% difference in CCS.[121] Hence it can be said that the observed shoulder in the peak may be a conformer as proposed by a previous study[120] due to flexibility in structure.

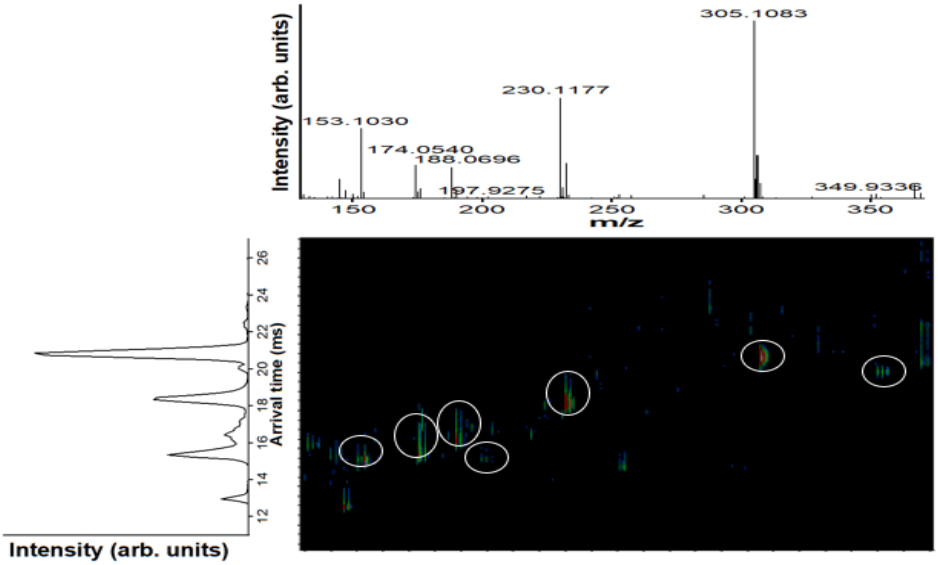

Figure 3.4: 2-Dimensional **s**eparation of a mixture of parent pesticides and degradation products using LC-IM-MS

Also, chlorpyrifos and TCP were separated and identified in the pesticide mixture. 349.9336 and 197.9275 were the observed accurate mass measurements for chlorpyrifos and its degradation product respectively. CCS values of 165.6 ± 0.4 $Å^2$ and 132.0 ± 0.5 $Å^2$ can be used as additional molecular descriptors for further identification of both chlorpyrifos and TCP.

A previous study indicated that propazine and terbuthylazine co-eluted in the LC.[121] In the optimized method, the constitutional isomers in the mixture (propazine and terbuthylazine), were separated in the LC. Accurate mass measurement could not be used in the identification of the separated peaks due to the same m/z. Since they differ in structure (two isopropyl groups in propazine while terbuthylazine had a tert-butyl group and an ethyl group), they interacted differently with the buffer gas resulting in different CCS values.[23, 59] The CCS value obtained for propazine was 155.1 ±0.3 $Å^2$ and that of terbuthylazine was 153.8 ±0.3 $Å^2$.

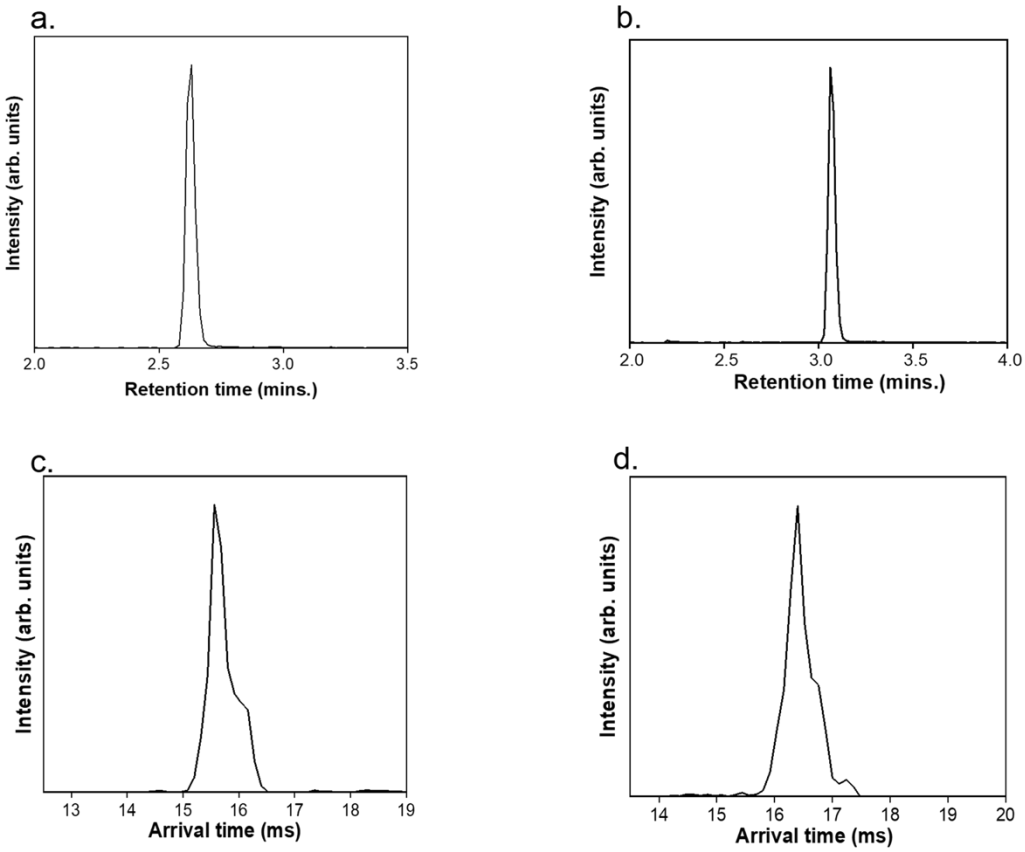

Figure 3.5: LC Chromatogram and IM spectra of degradation products. a. chromatogram of atrazine-desisopropyl b. chromatogram of atrazine-desethyl c. IM spectrum of atrazine-desisopropyl d. IM spectrum of atrazine-desethyl

3.3.1.3 Identification of pesticides and their degradation products in a spiked spinach sample by LC-IM-MS

A mixture of the pesticides and their corresponding degradation products (Table 3.3) was spiked into an organic spinach extract. The extract was initially screened for the presence of the analytes in the pesticide mixture before spiking. None of the analytes present in the pesticide mixture was found in the extract. The parent pesticides and degradation products were successfully separated in the LC due to the difference in their polarities as shown in Figure 3.6a. It was observed that, all the degradation products eluted earlier before the parent pesticides. This is due to the high polarity of degradation products than parent pesticides as reported in a previous work.[72] Further separation

was performed using the IM-dimension (Figure 3.6b). Due to the difference in molecular size and shape of analytes, they were differentiated using their CCS values. All analytes were identified using their accurate mass measurements except for the isomers (Figure 3.6c). The isomers (propazine and terbuthylazine) were identified using their retention times in combination with their CCS values due to their structural difference. Propazine eluted earlier than terbuthylazine indicating it being more polar than its isomer. In contrast, in the IM, propazine arrived later than terbuthylazine. A close look at the structure of both isomers, it can be seen that the two isopropyl groups attached at the sides of propazine makes it more open compared to terbuthylazine which has a tertbutyl and ethyl group attached to the sides. Due to the complementary separation of the LC and IM, the isomers were easily differentiated.

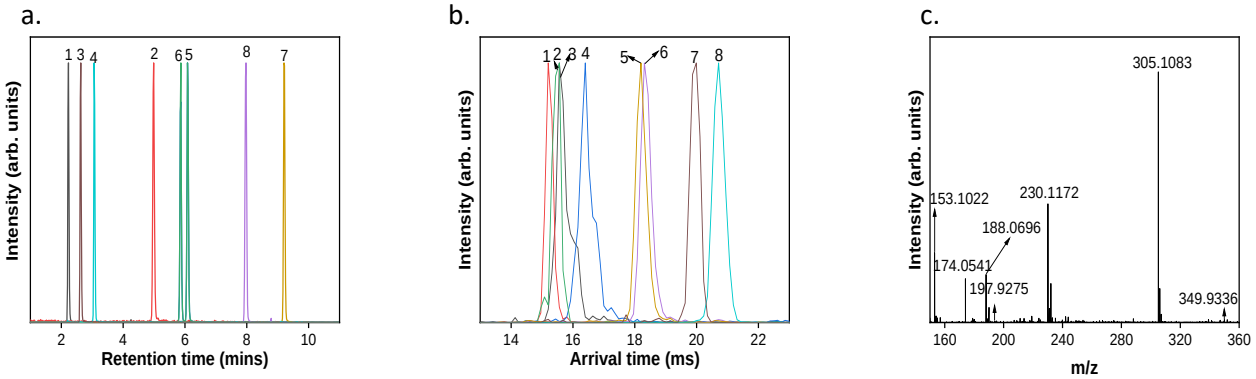

Figure 3.6: Identification of parent pesticides and degradation products in spinach extract using LC-IM-MS a. LC chromatogram b. IM spectrum c. Mass spectrum

3.3.2 Screening of Parent pesticides and degradation products using PS-IM-MS

3.3.2.1 Selection of spray solvent

Isopropyl alcohol (IPA), acetonitrile (ACN) and methanol (MeOH) were evaluated to ascertain their effects on the arrival time of ions (Figure 2). In this work, propazine sample was utilized for the investigation. Different arrival times of the propazine were observed when different solvents were used. Arrival time of 19.94 ± 0.4 ms was obtained when ACN was used as a spray solvent.

Two peaks were observed when IPA was utilized as spray solvent with arrival times of 18.68 ± 0.3 ms and 20.20 ± 0.4 (Figure 3.7). 18.71 ± 0.3 ms arrival time was observed when methanol was used as spray solvent. The increased arrival time observed when ACN was used as spray solvent was attributed to the incomplete desolvation of the analyte. A desolvated peak and incomplete desolvated peak was observed in the IM spectrum when IPA was utilized. The best solvated ion was observed when MeOH was used (in comparison to when AJS was in use). This is because methanol is more volatile compared to ACN and IPA. Boiling points of the three solvents are 64.7°C, 82.5°C and 82 °C for MeOH, IPA and ACN respectively. The lesser the boiling point of a solvent, the more volatile it is.[122] Hence a more desolvated ion was observed when methanol was used as spray solvent due to the fact that methanol is more volatile compared to ACN and IPA.[123] This was confirmed by initially varying the spray solvent volume and distance from the IM-MS inlet. Incompletely desolvated ions were formed when spray solvent of more than 10 µl was applied indicating more solvation of ion as more solvent was added. Also, paper distance less than 7 mm from IM-MS inlet showed incomplete desolvation of the analyte whereas distance from 7 mm and beyond showed complete desolvation. This is due to the fact that the analyte gets more desolvated as it travels through the longer distance (7 – 9 mm) until it gets to the IM-MS inlet as compared to the shorter distance (6mm and below). Therefore, we think that further optimizing the spray conditions can lead to the observation of a single IM-peak regardless of the chosen spray solvent as reported previously.[59] Hence, methanol was chosen as the spray solvent in this study.

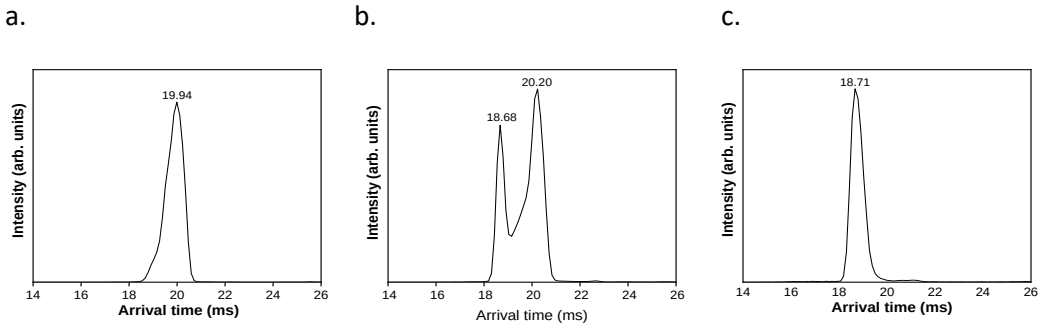

Figure 3.7: Effect of spray solvent of arrival time of analyte a. acetonitrile b. isopropyl alcohol c. methanol. Same conditions were utilized for the comparison study.

Table 3.4: Theoretical and experimental CCS of the pesticides and degradation products

Analyte	Adduct	Theo. CCS	Exp. CCS	%Error
Diazinon	$[M+H]^+$	175.2	172.8 ± 0.5	1.4
IMP	$[M+H]^+$	133.1	131.7 ± 0.5	1.1
Propazine	$[M+H]^+$	157.5	155.1 ± 0.3	1.5
DEA	$[M+H]^+$	143.7	139.9 ± 0.2	2.8
Terbuthylazine	$[M+H]^+$	156.6	153.8 ± 0.3	1.8
DIA	$[M+H]^+$	138.9	134.0 ± 0.2	3.6
Chlorpyrifos	$[M+H]^+$	161.2	164.8 ± 0.4	2.1
TCP	$[M-H]^-$	116.0	131.5 ± 0.3	11.7

3.3.2.2 Analysis of parent pesticides and degradation products in pesticide mixture

A mixture was prepared using the four parent pesticides and their degradation products and analyzed using PS-IM-MS in both positive and negative modes. Seven (all four parent pesticides and three degradation products) out of the eight analytes were detected in the positive mode. 3,5,6-trichloro-2-pyridinol was not detected in the positive mode. Nevertheless, it was detected significantly in the negative mode (see Figure A3). This could be ascribed to the presence of the three electronegative Cl atoms in its structure which draw the electron density more towards themselves and the N participating in resonance making the N atom not readily available to accept protons. However, the hydroxyl group in the structure can easily be deprotonated hence the detection of the analyte in the negative mode.

Accurate mass measurement of 305.1083 and 153.1030 were utilized for the identification of diazinon and IMP. Since the structures of both parent pesticide and degradation product are different, they interacted differently with the buffer gas in the drift tube resulting in different arrival times leading to distinctive CCS values. CCS values of 131.7 ± 0.5 $Å^2$ and 172.8 ± 0.5 $Å^2$ were obtained for IMP and diazinon respectively. There were no significant differences between the observed CCS values of all the analytes spiked into the spinach in comparison to the CCS values of the analytes in solvents. CCS value of 173.15 $Å^2$ is reported for diazinon elsewhere[118] which is similar to the obtained value with a percentage difference of 0.2%. The CCS values were used for further identification of the analytes. In the computational calculations, six different protonation sites were considered for diazinon (see Table A2). From this calculation, 0.0 kcal/mol and 0.2 kcal/mol relative energies were obtained for two of the protomer structures. The remaining five protomers are observed to have relative energies above 6 kcal/mol. From a previous theoretical study,[112] structures with relative energy of ≤ 6 kcal/mol are considered stable. Based on this analogy, the two protomers with relative energies below ≤ 6 kcal/mol are considered the most stable structures out of the six. A higher level of theory, MP2/6-311++G(d,p) was used for the two stable structures obtained to verify their stability. Nekkanti and Martin[112] investigated cationic pterin. For their obtained tautomers of ≤ 6 kcal/mol energy differences, they utilized a higher level of theory; MP2/6-31+G(d,p) to support the calculated energies. Energy difference of 0.6 kcal/mol was obtained for the two stable structures of diazinon when a higher level of theory; MP2/6-311++G(d,p) was used. The obtained energy for the two structures confirmed their stability (Table A1). The percentage difference between the CCS of both protomers is ~0.3%. This indicates the possibility of the two protomer structures observed simultaneously in experiment, hence seen as a single peak in the experiment. For IMP, three sites were considered for protonation (see Table A1)

and two of the structures gave relative energies above 6 kcal/mol with the third structure giving relative energy of 0.0 kcal/mol. Using the most stable theoretical structures (0.0 kcal/mol) of both diazinon and IMP, the theoretical values were found to be within the acceptable error margin reported elsewhere.[124]

Further noted, the US EPA concluded on the addition of propazine and its degradation product atrazine-desethyl to the cumulative risk assessment of triazines.[125] This was due to their toxicity to the neuroendocrine which may lead to developmental and reproductive changes. A lot of studies have focused on the collision induced dissociation (CID) of propazine for its identification without considering its degradation product DEA.[126] In the present study, propazine and atrazine-desethyl in the pesticide mixture are identified using their accurate mass measurements and CCS values (Table 3.4). Bauer and co-workers[119] utilized travelling wave IMS-QTOF for the separation of some isomeric triazines including propazine. In this study, the CCS value of propazine was 155.1 ± 0.3 $Å^2$ while Bauer and comrades reported CCS of 155.5 $Å^2$. The % difference in CCS between this study and the previous study is ~0.3% showing similarity in the reported values. Three protomers with relative energy of 0.0 kcal/mol, 0.4 kcal/mol and 4.7 kcal/mol relative energies are obtained. Two of the three protomers are observed to be stable when the higher level of theory was used (Figure A1). The structure with the relative energy of 4.7 kcal/mol was observed to have relative energy of 10.8 kcal/mol when a higher level of the theorey was utilized revealing its instability. Similar trend is observed in DEA with two of the three protomer structures observed to be relatively stable (Figure A1). Hence the CCS values of the two most stable structures of propazine were 157.71 $Å^2$ and 157.98 $Å^2$ while that of DEA were 143.78 $Å^2$ and 144.1 $Å^2$ respectively.

Terbuthylazine is a triazine pesticide used as a substitute for atrazine which is known to cause many detrimental health effects.[127] However, Tariba Lovakovi et al.[128] reported that terbuthylazine and its degradation products could be a possible cause of oxidative stress and cause damage to the human DNA. In this study, terbuthylazine and DIA are analyzed in the pesticide mixture. Accurate mass measurement of 230.1177 and CCS value of 153.8 ± 0.3 $Å^2$ were used to identify terbuthylazine (see Table 3.4). From the theoretical study, three stable structures of terbuthylazine with relative energies of 0.0 kcal/mol, 0.6 kcal/mol and 5.0 kcal/mol are obtained. When the higher level of theory was used, two of the protomers were revealed to be stable with the third being relatively unstable (Table A1). The trend observed with the MP2/6-311++G(d,p) level of theory is similar to what is observed with B3LYP/6-31G(d,p) with the higher energy one among the three having a higher energy of 6.4 kcal/mol (Figure A1). Results from the computational study revealed three stable protomers of DIA (see Figure A1) using B3LYP/6-31G(d,p) and two stable protomers when a higher level of theory was used (Figure A1). 156.6 $Å^2$ and 157.3 $Å^2$ CCS values were obtained for terbuthylazine while 138.9 $Å^2$ and 139.3 $Å^2$ were obtained for its degradation product respectively.

The parent pesticide, chlorpyrifos and its degradation product (TCP) are persistent pesticides in the environment.[129] Due to the endocrine disrupting function of chlorpyrifos, its exposure can lead to reproductive and developmental neurotoxicity in mammals.[130]A recent study revealed that chlorpyrifos and its degradation products disrupts progesterone signaling by their interference with the binding of progesterone to the human progesterone receptor.[131] Armstrong et al[132] utilized LC-MS/MS method in the determination of the level of chlorpyrifos in air. In their work, the parent pesticide was the only focus meanwhile some of the degradation products could also cause problems upon exposure. Caceres and co-workers reported that the toxicity of TCP to *Deinacrida*

carinata in cladoceran water was higher compared to the parent pesticide; chlorpyrifos.[133] In the present study, chlorpyrifos and TCP were separated and identified in the pesticide mixture. 349.9336 and 195.9136 were the observed accurate mass measurements for chlorpyrifos and its degradation product respectively. CCS values of 165.6 ± 0.4 $Å^2$ and 132.0 ± 0.5 $Å^2$ can be used as additional molecular descriptors for further identification of both chlorpyrifos and TCP. Computational calculation revealed one stable structure for the parent pesticide and its degradation product (Table A1).

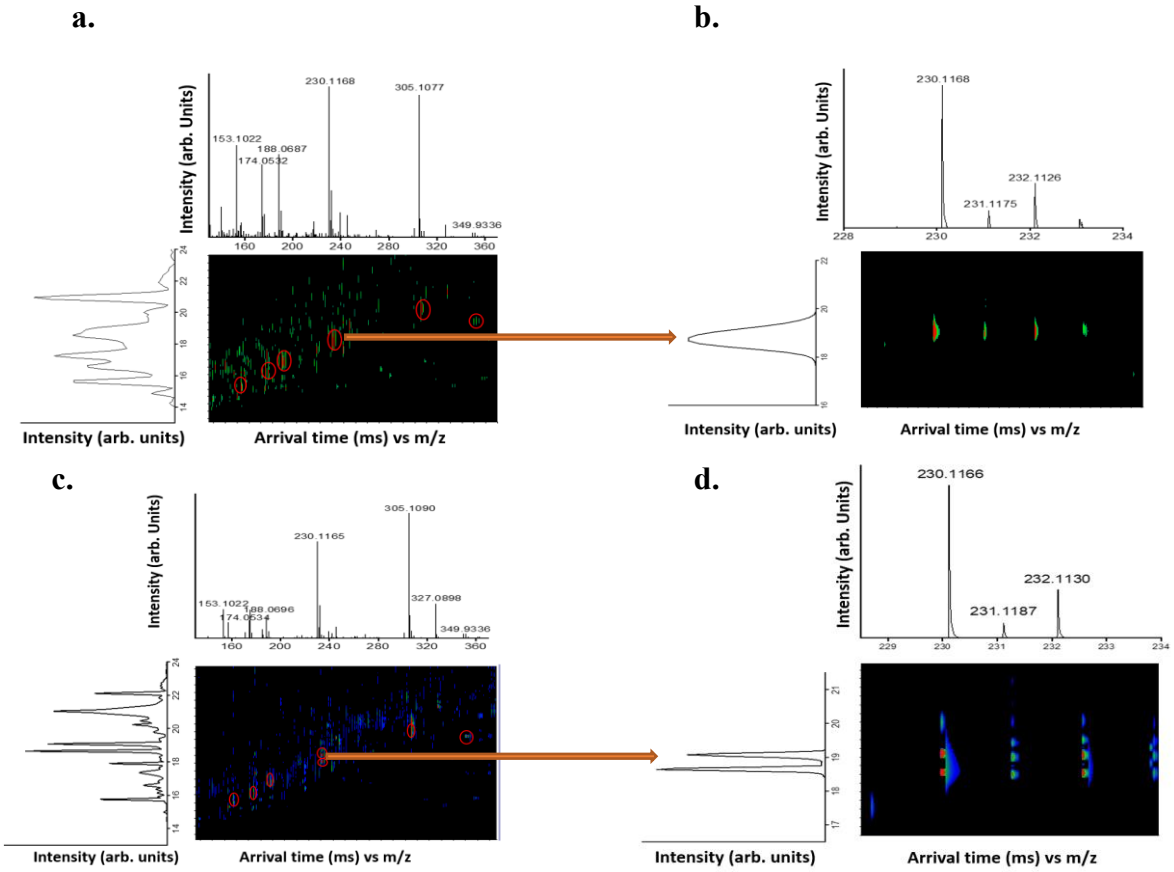

Figure 3.9: Heat map for the separation and identification of parent pesticides and degradation products in a mixture a. Conventional PS-IM-MS b. Single peak for propazine and terbuthylazine c. PS-IM-MS multiplexed mode d. resolved propazine and terbuthylazine peaks

In summary, all analytes were identified with their accurate mass measurements with the exception of the propazine and terbuthylazine. The constitutional isomers differ in structure with propazine

having two isopropyl groups and terbuthylazine having a tert-butyl group and an ethyl group.[59] A single peak was observed for both isomers in the mass and drift spectra since they have similar arrival times and same m/z (Figures 3.9 a and b). The mixture was further analyzed using PS-IM-MS in multiplexing mode (Figure 3.9 c and d). A demultiplexer was utilized for initial demultiplexing of the obtained data and a further demultiplexing was performed using high resolution demultiplexer (HRdm) software. After demultiplexing using the HRdm, propazine and terbuthylazine were resolved. The CCS value obtained for propazine was 155.1 ±0.3 $\dot{A}^2$ and that of terbuthylazine was 153.8 ±0.3 $\dot{A}^2$. From the theoretical calculation, CCS values of 157.7 $\dot{A}^2$ and 156.6 $\dot{A}^2$ were obtained for propazine and terbuthylazine respectively with a difference of 1.1 $\dot{A}^2$ which is similar to the experimental CCS values with a difference of 1.3 $\dot{A}^2$. Similar results were reported on structural isomers (sodiated monomers of testosterone and dehydroepiandrosterone) that differ in the position of their hydroxyl/ketone groups and double bond.[134] The reported CCS values showed minimal separation of 1.2 $\dot{A}^2$.[134] Also, two isomeric metabolites, citrate and isocitrate were differentiated by their CCS of 143.1 $Å^2$ and 142.7 $Å^2$ respectively (0.4 $Å^2$ difference).[78]

3.3.2.3 Identification of pesticides and their degradation products in a spiked spinach sample by PS-IM-MS

The conventional method that is typically used for the screening of pesticides and their degradation products is LC-MS/MS.[132, 135] However, this method is time consuming and requires significant volume of solvents leading to generation of a lot of waste. Previous studies have utilized paper spray mass spectrometry for the screening of pesticides.[4a, 57a] However to the best of my knowledge, none of these studies included isomers as well as degradation products of the parent pesticides. In a previous study, the promising ability of PS-IM-MS for rapid screening of pesticides

in agricultural products was shown.[59] In the current study, a pesticide mixture was spiked into an organic spinach extract to form a contaminated spinach sample. The organic spinach extract was initially screened for the presence of the analytes before spiking to ensure none of the analytes were present. The extract was then spiked with the pesticide mixture (100 ppb) for analysis. Upon screening the contaminated spinach extract, the parent pesticides and degradation products were detected. They were separated in using ion mobility due to the difference in their structural shape and size. All analytes were identified using their accurate mass measurements except for the isomers. With the use of multiplexing and the HRdm, the isomers (propazine and terbuthylazine) were separated and identified using their CCS values (Figure 4.0). This technique is rapid and efficient for the screening of parent pesticides and their degradation products in agricultural produce. It must be noted that similar CCS values of analytes were observed in spiked spinach sample in comparison with analytes in pure solvent.

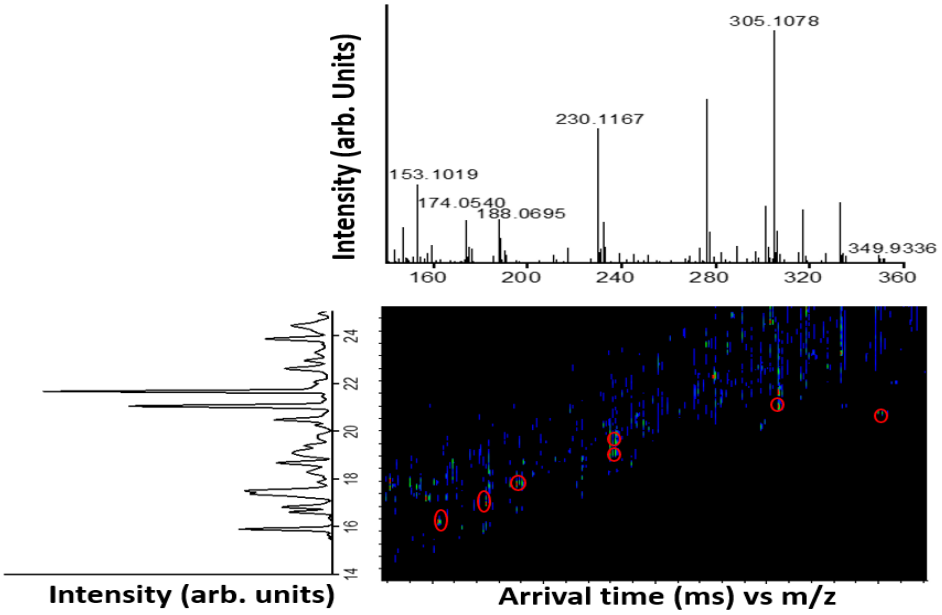

Figure 4.0: Heat map of screened spinach extract showing separation and identification

3.4 Conclusion

In summary, this work reports the successful screening of isomeric and non-isomeric parent pesticides and their degradation products using LC-IM-MS and a rapid method, PS-IM-MS. A combination of parent pesticides and degradation products were identified and differentiated using their retention times, accurate mass measurements, and CCS values when LC-IM-MS was utilized. PS-IM-MS allows the rapid separation and identification of the parent pesticides and their degradation products in complex matrix such as spinach sample with little sample preparation. From the generated contaminated spinach sample, all analytes were detected and identified. This method is rapid and involves less solvent and low generation of waste compared to the conventional LC-MS/MS which is mostly used for the identification of pesticides. Unique molecular descriptor, CCS value is obtained from the IM experiment which aids in structure identification together with computational calculations. Single field approach was utilized for the determination of the CCS values. Comparing CCS values obtained from experiment to DFT calculations, the plausible experimental structures are reported. In addition, the use of multiplexing and a high resolution demultiplexer aided in the separation of the two isomers in the mixture. The use of ambient ionization coupled with higher resolution IM platforms would facilitate its usage in different fields.

4.0 **References**

[1] M. A. Grayson, *Measuring mass: from positive rays to proteins*, Chemical Heritage Foundation, **2002**, p.

[2] J. Griffiths, *Anal. Chem* **2008**, *80*, 5678-5683.

[3] P. Hemmersbach, *Journal of mass spectrometry* **2008**, *43*, 839-853.

[4] a) I. N. L. Ana Carolina Martins Moura, Claudio Fernandes Cardoso, and I. P. Abadia dos Reis Nascimento, Boniek Gontijo Vaz, *Food chemistry* **2020**, 125938; b) R. Borisov, L. Kulikova and V. Zaikin, *Petroleum Chemistry* **2019**, *59*, 1055-1076; c) A. Demelenne, G. Nys, C. Nix, J. C. Fjeldsted, J. Crommen and M. Fillet, *Analytica Chimica Acta* **2021**, 339297; d) R. Fernández-Maestre and M. Doerr in *On the Separation of Enantiomers by Drift Tube Ion Mobility Spectrometry*, *Vol.* **2021**; e) M. T. Hetmanski, R. Fussell, M. Godula and H.-J. Hübschmann, **2013**, 473; f) Y. P. Ho and P. M. Reddy, *Mass spectrometry reviews* **2011**, *30*, 1203-1224.

[5] C. G. de Koster and P. J. Schoenmakers in *History of liquid chromatography—mass spectrometry couplings*, Elsevier, **2020**, pp. 279-295.

[6] A. Nuñez, Y. Sapozhnikova and S. J. Lehotay, *Toxics* **2018**, *6*.

[7] S. Knoll, T. Rösch and C. Huhn, *Analytical and bioanalytical chemistry* **2020**, 1-17.

[8] a) C. Yu, D. Hao, Q. Chu, T. Wang, S. Liu, T. Lan, F. Wang and C. Pan, *Food chemistry* **2020**, *321*, 126657; b) Y. Shin, J. Lee, J. Lee, J. Lee, E. Kim, K.-H. Liu, H. S. Lee and J.-H. Kim, *Journal of agricultural and food chemistry* **2018**, *66*, 3550-3560; c) T. B. Rodrigues, D. R. Morais, V. A. Gianvecchio, E. M. Aquino, R. L. Cunha, M. A. Huestis and J. L. Costa, *Journal of Analytical Toxicology* **2020**; d) G. L. Marques, A. A. Siqueira, V. S. Minassa, M. D. Peres, F. S. Pelição and K. N. Sampaio, *Journal of Chromatography B* **2018**, *1097*, 44-53; e) P. S. Fišerová, J. Kohoutek, C. Degrendele, M. A. Dalvie and J. Klánová, *Journal of Chromatography B* **2021**, *1166*, 122542.

[9] T. Baygildiev, M. Vokuev, A. Braun, I. Rybalchenko and I. Rodin, *Journal of Chromatography B* **2021**, *1162*, 122452.

[10] a) M. Kresse, H. Drinda, A. Romanotto and K. Speer, *Journal of Chromatography B* **2019**, *1117*, 86-102; b) H. Puntscher, I. Cobankovic, D. Marko and B. Warth, *Food Control* **2019**, *102*, 157-165.

[11] C.-H. Chiang, H.-H. Lee, B.-H. Chen, Y.-C. Lin, Y.-Y. Chao and Y.-L. Huang, *Journal of food and drug analysis* **2019**, *27*, 439-450.

[12] Y. S. Chhonker, C. Edi and D. J. Murry, *Journal of pharmaceutical and biomedical analysis* **2018**, *151*, 84-90.

[13] J. Wang, C. Yang, J. Beck and D. Ghosh, *Thermo Scientific Application, Thermo Scientific: San Jose, CA, USA* **2016**.

[14] A. B. Kanu, P. Dwivedi, M. Tam, L. Matz and H. H. Hill Jr, *Journal of mass spectrometry* **2008**, *43*, 1-22.

[15] R. Cumeras, E. Figueras, C. E. Davis, J. I. Baumbach and I. Gràcia, *Analyst* **2015**, *140*, 1376.

[16] A. S. Guntner, B. Thalhamer, C. Klampfl and W. Buchberger, *Scientific Reports* **2019**, *9*, 1-10.

[17] G. A. Eiceman, Z. Karpas and H. H. Hill Jr, *Ion mobility spectrometry*, CRC press, **2005**, p.

[18] E. A. Mason and E. W. McDaniel, *NASA STI/Recon Technical Report a* **1988**, *89*, 15174.

[19] X. Zheng, N. A. Aly, Y. Zhou, K. T. Dupuis, A. Bilbao, V. L. Paurus, D. J. Orton, R. Wilson, S. H. Payne, R. D. Smith and E. S. Baker, *Chemical Science* **2017**, *8*, 7724-7736.

[20] a) S. M. Stow, T. J. Causon, X. Zheng, R. T. Kurulugama, T. Mairinger, J. C. May, E. E. Rennie, E. S. Baker, R. D. Smith, J. A. McLean, S. Hann and J. C. Fjeldsted, *Analytical Chemistry* **2017**, *89*, 9048-9055; b) M. Ekelöf, J. Dodds, S. Khodjaniyazova, K. P. Garrard, E. S. Baker and D. C. Muddiman, *Journal of the American Society for Mass Spectrometry* **2020**, *31*, 642-650.

[21] a) R. B. Lubertus Bijlsma, ⊥ Alberto Celma, Lauren Mullin, Gareth Cleland, Sara Stead, and a. J. V. S. Felix Hernandez, *Analytical chemistry* **2017**, *89*, 6583-6589; b) J. C. May, C. R. Goodwin, N. M. Lareau, K.

L. Leaptrot, C. B. Morris, R. T. Kurulugama, A. Mordehai, C. Klein, W. Barry, E. Darland, G. Overney, K. Imatani, G. C. Stafford, J. C. Fjeldsted and J. A. McLean, *Analytical Chemistry* **2014**, *86*, 2107-2116.
[22] K. M. Hines, J. C. May, J. A. McLean and L. Xu, *Analytical Chemistry* **2016**, *88*, 7329-7336.
[23] B. Donkor, O. Olajide and A. M. Hamid, *Proceedings of the 69th ASMS Conference on Mass Spectrometry and Allied Topics* (Philadelphia) **2021**.
[24] A. N. Hoofnagle and M. H. Wener, *Journal of Immunological Methods* **2009**, *347*, 3-11.
[25] R. S. Zhao, J. P. Yuan, T. Jiang, J. B. Shi and C. G. Cheng, *Talanta* **2008**, *76*, 956-959.
[26] Z. Ouyang and X. Zhang, *Analyst* **2010**, *135*, 659-660.
[27] J. B. Fenn, M. Mann, C. K. Meng, S. F. Wong and C. M. Whitehouse in *Electrospray ionization for mass spectrometry of large biomolecules*, *Vol. 246* **1989**, pp. 64-71.
[28] Z. Takáts, J. M. Wiseman, B. Gologan and R. G. Cooks, *Science* **2004**, *306*, 471-473.
[29] R. R. Steiner and R. L. Larson, *Journal of Forensic Sciences* **2009**, *54*, 617-622.
[30] a) E. Gurdak, F. M. Green, P. D. Rakowska, M. P. Seah, T. L. Salter and I. S. Gilmore, *Analytical Chemistry* **2014**, *86*, 9603-9611; b) Z. E. Lawton, A. Traub, W. L. Fatigante, J. Mancias, A. E. O'Leary, S. E. Hall, J. R. Wieland, H. Oberacher, M. C. Gizzi and C. C. Mulligan, *Journal of the American Society for Mass Spectrometry* **2017**, *28*, 1048-1059.
[31] C. L. Feider, A. Krieger, R. J. DeHoog and L. S. Eberlin, *Analytical chemistry* **2019**, *91*, 4266-4290.
[32] a) L.-H. Li, H.-Y. Hsieh and C.-C. Hsu, *Mass Spectrometry* **2017**, *6*, S0060-S0060; b) R. Chen, J. Deng, L. Fang, Y. Yao, B. Chen, X. Wang and T. Luan, *Trends in Environmental Analytical Chemistry* **2017**, *15*, 1-11; c) T. Acter, N. Uddin, N. N. Solihat and S. Kim, *Energy & Fuels* **2021**, *35*, 15545-15554.
[33] J. Liu, H. Wang, N. E. Manicke, J. M. Lin, R. G. Cooks and Z. Ouyang, *Analytical Chemistry* **2010**, *82*, 2463-2471.
[34] N. E. Manicke, B. J. Bills and C. Zhang, *Bioanalysis* **2016**, *8*, 589-606.
[35] a) R. D. Espy, N. E. Manicke, Z. Ouyang and R. G. Cooks, *Analyst* **2012**; b) R. D. Espy, S. F. Teunissen, N. E. Manicke, Y. Ren, Z. Ouyang, A. Van Asten and R. G. Cooks, *Analytical Chemistry* **2014**, *86*, 7712-7718; c) D. E. Damon, K. M. Davis, C. R. Moreira, P. Capone, R. Cruttenden and A. K. Badu-Tawiah, *Analytical Chemistry* **2016**, *88*, 1878-1884.
[36] Y. Ren, H. Wang, J. Liu, Z. Zhang, M. N. McLuckey and Z. Ouyang, *Chromatographia* **2013**, *76*, 1339-1346.
[37] J. McKenna, E. S. Dhummakupt, T. Connell, P. S. Demond, D. B. Miller, J. M. Nilles, N. E. Manicke and T. Glaros, *Analyst* **2017**, *142*, 1442-1451.
[38] E. L. Rossini, D. S. Kulyk, E. Ansu-Gyeabourh, T. Sahraeian, H. R. Pezza and A. K. Badu-Tawiah, *Journal of the American Society for Mass Spectrometry* **2020**, *31*, 1212-1222.
[39] J. Liu, H. Wang, R. G. Cooks and Z. Ouyang, *Analytical Chemistry* **2011**, *83*, 7608-7613.
[40] B. Hu, P. K. So, H. Chen and Z. P. Yao, *Analytical Chemistry* **2011**, *83*, 8201-8207.
[41] M. Y. M. Wong, H. W. Tang, S. H. Man, C. W. Lam, C. M. Che and K. M. Ng, *Rapid Communications in Mass Spectrometry* **2013**, *27*, 713-721.
[42] Z. Yu, L. C. Chen, M. K. Mandal, K. Yoshimura and S. Takeda, **2013**, 1612-1615.
[43] G. T. T. Gibson, R. D. Wright and R. D. Oleschuk, *Journal of Mass Spectrometry* **2012**, *47*, 271-276.
[44] a) B. J. Bills and N. E. Manicke, *Clinical Mass Spectrometry* **2016**, *2*, 18-24; b) C. Zhang and N. E. Manicke, *Analytical Chemistry* **2015**, *87*, 6212-6219.
[45] a) B. J. Bills, J. Kinkade, G. Ren and N. E. Manicke, *Forensic Chemistry* **2018**, *11*, 15-22; b) M. Sneha, M. T. Dulay and R. N. Zare, *International Journal of Mass Spectrometry* **2017**, *418*, 156-161.
[46] E. L. Rossini, D. S. Kulyk, E. Ansu-Gyeabourh, T. Sahraeian, H. R. Pezza and A. K. Badu-Tawiah, *Journal of the American Society for Mass Spectrometry* **2020**.
[47] C. Zhang, B. J. Bills and N. E. Manicke, *Bioanalysis* **2017**, *9*, 329-331.
[48] E. G. Gordeev, E. S. Degtyareva and V. P. Ananikov in *Analysis of 3D printing possibilities for the development of practical applications in synthetic organic chemistry*, *Vol. 65* **2016**, pp. 1637-1643.

[49] C. Vega, C. Spence, C. Zhang, B. J. Bills and N. E. Manicke, *Journal of the American Society for Mass Spectrometry* **2016**, *27*, 726-734.
[50] K. E. Yannell, K. R. Kesely, H. D. Chien, C. B. Kissinger and R. G. Cooks, *Analytical and Bioanalytical Chemistry* **2017**, *409*, 121-131.
[51] W. Zhou, Z. Yang, S. Huang, Z. Fang, B. Chen and M. Ma, *Journal of Pharmaceutical and Biomedical Analysis* **2019**, *171*, 158-163.
[52] L. Bartella, L. Di Donna, A. Napoli, C. Siciliano, G. Sindona and F. Mazzotti, *Food Chemistry* **2019**, *278*, 261-266.
[53] C. A. Chamberlain, V. Y. Rubio and T. J. Garrett, *Analytical Chemistry* **2019**, *91*, 4964-4968.
[54] R. R. Ramalho, L. C. da Silva, L. I. Maciel, I. Pereira, A. d. R. Nascimento, R. C. Simas and B. G. Vaz, *Analytical and Bioanalytical Chemistry* **2020**, *412*, 5389-5396.
[55] J. Zhao, Y. Zheng and Z. Zhang, *Analytical Methods* **2020**, *12*, 1926-1934.
[56] a) T. Guo, W. Yong and Y. Dong, *Food Analytical Methods* **2019**, *12*, 1208-1217; b) T. Guo, Z. Zhang, K. E. Yannell, Y. Dong and R. G. Cooks, *Analytical Methods* **2017**, *9*, 6273-6279; c) A. C. M. Moura, I. N. Lago, C. F. Cardoso, A. dos Reis Nascimento, I. Pereira and B. G. Vaz, *Food chemistry* **2020**, *310*, 125938.
[57] a) Y.-C. L. Kuan-Hong Chen, Fuu Sheu, Che-Hsin Lin, *Food Chemistry* **2021**, 130305; b) A. C. M. Moura, I. N. Lago, C. F. Cardoso, A. dos Reis Nascimento, I. Pereira and B. G. Vaz, *Food Chemistry* **2020**, *310*, 1-6; c) S. L. Reeber, S. Gadi, S. B. Huang and G. L. Glish, *Analytical Methods* **2015**.
[58] N. E. Manicke and M. Belford, *Journal of the American Society for Mass Spectrometry* **2015**.
[59] O. E. Olajide, B. Donkor and A. M. Hamid, *Journal of the American Society for Mass Spectrometry* **2021**.
[60] P. Chawla, R. Kaushik, V. S. Swaraj and N. Kumar, *Environmental nanotechnology, monitoring & management* **2018**, *10*, 292-307.
[61] a) M. Rani, U. Shanker and V. Jassal, *Journal of environmental management* **2017**, *190*, 208-222; b) V. Terziev and S. Petkova-Georgieva, *IJASOS-International E-journal of Advances in Social Sciences* **2019**, *5*.
[62] J. Kaushal, M. Khatri and S. K. Arya, *Ecotoxicology and Environmental Safety* **2021**, *207*, 111483.
[63] J. R. Reigart and J. R. Roberts, *Organophosphates*, **2013**, p. 43-55.
[64] E. A. Jara and C. K. Winter, *International Journal of Food Contamination* **2019**, *6*, 1-8.
[65] C. C. Lerro, S. Koutros, G. Andreotti, M. C. Friesen, M. C. Alavanja, A. Blair, J. A. Hoppin, D. P. Sandler, J. H. Lubin and X. Ma, *Occupational and environmental medicine* **2015**, *72*, 736-744.
[66] a) S. K. Sagiv, M. H. Harris, R. B. Gunier, K. R. Kogut, K. G. Harley, J. Deardorff, A. Bradman, N. Holland and B. Eskenazi, *Environmental health perspectives* **2018**, *126*, 047012; b) M. Jokanović, *Toxicology* **2018**, *410*, 125-131.
[67] K. Jaga and C. Dharmani, *Revista Panamericana de Salud Publica/Pan American Journal of Public Health* **2003**, *14*, 171-185.
[68] S. Karami and A. Rafiee, *Genetika* **2020**, *52*, 1031-1040.
[69] K. Jaga and C. Dharmani, *Environmental Health and Preventive Medicine* **2006**, *11*, 102-107.
[70] H. John, M. Siegert, A. Kranawetvogl and H. Thiermann, *Rapid Communications in Mass Spectrometry* **2019**, *33*, 259-271.
[71] G. Georgiadis, C. Mavridis, C. Belantis, I. Zisis, I. Skamagkas, I. Fragkiadoulaki, I. Heretis, V. Tzortzis, K. Psathakis and A. Tsatsakis, *Toxicology* **2018**, *406*, 129-136.
[72] J. F. García-Reyes, A. Molina-Díaz and A. R. Fernández-Alba, *Analytical Chemistry* **2007**, *79*, 307-321.
[73] a) F. Allen, A. Pon, R. Greiner and D. Wishart, *Analytical Chemistry* **2016**, *88*, 7689-7697; b) J. Cautereels in *Quantum chemical mass spectrometry : detailed insight into the fragmentation behaviour of small organic molecules , peptides and lipids*, *Vol.* **2019**; c) S. Wang, T. Kind, D. J. Tantillo and O. Fiehn, *Journal of Cheminformatics* **2020**, *12*, 63.
[74] M. C. Hamilton, *Environmental Forensics: Contaminant Specific Guide* **2010**, 143.

[75] a) C. Ruttkies, E. L. Schymanski, S. Wolf, J. Hollender and S. Neumann, *Journal of cheminformatics* **2016**, *8*, 1-16; b) C. Ruttkies, S. Neumann and S. Posch, *BMC bioinformatics* **2019**, *20*, 1-14.
[76] M. J. T. Frisch, G. W.; Schlegel, H. B.; Scuseria, G. E.; Robb, M. A.; Cheeseman, J. R.; Scalmani, G.; Barone, V.; Petersson, G. A.; Nakatsuji, H.; Li, X.; Caricato, M.; Marenich, A. V.; Bloino, J.; Janesko, B. G.; Gomperts, R.; Mennucci, B.; Hratchian, H. P.; Ortiz, J. V.; Izmaylov, A. F.; Sonnenberg, J. L.; Williams-Young, D.; Ding, F.; Lipparini, F.; Egidi, F.; Goings, J.; Peng, B.; Petrone, A.; Henderson, T.; Ranasinghe, D.; Zakrzewski, V. G.; Gao, J.; Rega, N.; Zheng, G.; Liang, W.; Hada, M.; Ehara, M.; Toyota, K.; Fukuda, R.; Hasegawa, J.; Ishida, M.; Nakajima, T.; Honda, Y.; Kitao, O.; Nakai, H.; Vreven, T.; Throssell, K.; Montgomery, J. A., Jr.; Peralta, J. E.; Ogliaro, F.; Bearpark, M. J.; Heyd, J. J.; Brothers, E. N.; Kudin, K. N.; Staroverov, V. N.; Keith, T. A.; Kobayashi, R.; Normand, J.; Raghavachari, K.; Rendell, A. P.; Burant, J. C.; Iyengar, S. S.; Tomasi, J.; Cossi, M.; Millam, J. M.; Klene, M.; Adamo, C.; Cammi, R.; Ochterski, J. W.; Martin, R. L.; Morokuma, K.; Farkas, O.; Foresman, J. B.; Fox, D. J. in *Gaussian 16, Revision C.01*, *Vol.* Gaussian, Inc., Wallingford CT, **2016**.
[77] B. D. D. a. J. R. Schmidt, *Journal of chemical theory and computation* **2012**, *8*, 1902-1911.
[78] D. Böck, A. Beuchel, R. Goddard, A. Richter, P. Imming and R. W. Seidel, *Structural Chemistry* **2021**, *32*, 989-996.
[79] A. Halder, S. Bhattacharya, A. Datta, D. Bhattacharyya and A. Mitra, *Physical Chemistry Chemical Physics* **2015**, *17*, 26249-26263.
[80] D. P. Demarque, A. E. M. Crotti, R. Vessecchi, J. L. C. Lopes and N. P. Lopes in *Fragmentation reactions using electrospray ionization mass spectrometry: An important tool for the structural elucidation and characterization of synthetic and natural products*, *Vol. 33* Royal Society of Chemistry, **2016**, pp. 432-455.
[81] S. A. A. Sadat, V. Ilbeigi, Y. Valadbeigi and M. Soleimani, *International Journal for Ion Mobility Spectrometry* **2020**, *23*, 127-131.
[82] a) R. Bravo, W. J. Driskell, R. D. Whitehead, L. L. Needham and D. B. Barr, *Journal of Analytical Toxicology* **2002**, *26*, 245-252; b) M. B. Colovic, V. M. Vasi, M. M. Gaji and D. Z. Krsti, *Toxicology Letters* **2015**, *233*, 29-37.
[83] P. Wright, A. Alex, T. Nyaruwata, T. Parsons and F. Pullen, *Rapid Communications in Mass Spectrometry* **2010**, *24*, 1025-1031.
[84] J. D. Barr, A. J. Bell, M. Bird, J. L. Mundy, J. Murrell, C. M. Timperley, P. Watts and F. Ferrante, *Journal of the American Society for Mass Spectrometry* **2005**, *16*, 515-523.
[85] P. Wright, A. Alex and F. Pullen, *Rapid Communications in Mass Spectrometry* **2016**, *30*, 1163-1175.
[86] Z. He, L. Zhao, X. Liu and Y. Xu, *Journal of Chromatography A* **2020**, *1633*, 461637.
[87] E. M. Thurman, I. Ferrer, O. J. Pozo, J. V. Sancho and F. Hernandez, *Rapid Communications in Mass Spectrometry* **2007**, *21*, 3855-3868.
[88] D. Kaushik and G. Bansal, *Journal of pharmaceutical analysis* **2015**, *5*, 285-295.
[89] a) V. A. Muckoya, P. B. Njobeh, P. N. Nomngongo and J. C. Ngila, *Chromatographia* **2020**, *83*, 373-383; b) S. N. Sinha, *American Journal of Analytical Chemistry* **2011**, *02*, 511-521.
[90] Y. Lee, Y.-J. Kim, M. S. I. Khan and Y.-C. Na, *Journal of Separation Science* **2020**, *43*, 4047-4057.
[91] I. Ferrer and E. M. Thurman, *Journal of Chromatography A* **2007**, *1175*, 24-37.
[92] V. N. Kouloumbos, D. F. Tsipi, A. E. Hiskia, D. Nikolic and R. B. van Breemen, *Journal of the American society for mass spectrometry* **2003**, *14*, 803-817.
[93] a) A. Sharma, V. Kumar, B. Shahzad, M. Tanveer, G. P. S. Sidhu, N. Handa, S. K. Kohli, P. Yadav, A. S. Bali and R. D. Parihar, *SN Applied Sciences* **2019**, *1*, 1-16; b) L. Jiang, K. Gu, R. Liu, S. Jin, H. Wang and C. Pan, *SN Applied Sciences* **2019**, *1*, 1-9.
[94] a) A. Dragus, M. S. Beldean-Galea, R. Mihaiescu, T. Mihaiescu and D. Ristoiu, *Environmental Engineering and Management Journal* **2012**, *11*, 319-323; b) H. M. LeBaron, J. E. McFarland and O. C. Burnside, *The triazine herbicides* **2008**, *50*, 163-174.

[95] L. F. R. Vasconcellos, A. C. Leite and O. J. M. Nascimento, *Arquivos de Neuro-Psiquiatria* **2002**, *60*, 1003-1007.
[96] a) G. M. Calaf, *Seminars in Cancer Biology* **2021**; b) G. M. Calaf, T. C. Bleak and D. Roy, *Oncology Reports* **2021**, *45*, 1-1.
[97] E. L. Robb and M. B. Baker, *StatPearls* **2017**.
[98] D. Kathuria, M. Bhattu, M. Verma and B. K. Billing, *Analytical Methods* **2022**.
[99] a) P. Liu, L. Chen and H. Zhang, *Journal of Immunology Research* **2018**; b) E. Vivier, E. Tomasello, M. Baratin, T. Walzer and S. Ugolini, *Nature Immunology* **2008**, *9*, 503-510.
[100] M. M. Whalen, B. G. Loganathan, N. Yamashita and T. Saito, *Chemico-Biological Interactions* **2003**, *145*, 311-319.
[101] U. FDA in *Pesticide Residue Monitoring Program Fiscal Year 2015 Pesticide Report*, *Vol.* **2015**.
[102] a) Z. Ayhan, O. Esturk and Y. Yakar, *J Food Sci Technol* **2014**, *51*, 458-466; b) D. Tran, K. C. Hyland, S. Roberts, S. Krepich, P. Winkler, C. Butt and C. Borton, *Sciex Tech. Note* **2017**, 1-9.
[103] M.-a. Zhao, H. Gu, C.-J. Zhang, I.-H. Jeong, J.-H. Kim and Y.-Z. Zhu, *RSC Advances* **2020**, *10*, 19659-19668.
[104] L. D. Karalliedde, P. Edwards and T. C. Marrs, *Food and Chemical Toxicology* **2003**, *41*, 1-13.
[105] M. Čolović, D. Krstić, S. Petrović, A. Leskovac, G. Joksić, J. Savić, M. Franko, P. Trebše and V. Vasić, *Toxicology Letters* **2010**, *193*, 9-18.
[106] a) S. Biswas, R. Mondal, A. Mukherjee, M. Sarkar and R. K. Kole, *Food Chemistry* **2019**, *272*, 559-567; b) H. V. Botitsi, S. D. Garbis, A. Economou and D. F. Tsipi1, *Mass Spectrometry Reviews* **2011**, *30*, 907- 939; c) R. M. González-Rodríguez, R. Rial-Otero, B. Cancho-Grande and J. Simal-Gándara, *Journal of Chromatography A* **2008**, *1196-1197*, 100-109; d) F. Hernández, J. V. Sancho, M. Ibáñez and S. Grimalt, *TrAC - Trends in Analytical Chemistry* **2008**, *27*, 862-872; e) F. Hernández, J. V. Sancho and O. J. Pozo, *Rapid Communications in Mass Spectrometry* **2002**, *16*, 1766-1773; f) M. D. Hernando, C. Ferrer, M. Ulaszewska, J. F. García-Reyes, A. Molina-Díaz and A. R. Fernández-Alba, *Analytical and Bioanalytical Chemistry* **2007**, *389*, 1815-1831; g) M. G. López, R. J. Fussell, S. L. Stead, D. Roberts, M. McCullagh and R. Rao, *Journal of Chromatography A* **2014**, *1373*, 40-50; h) D. Ortelli, P. Edder and C. Corvi, *Analytica Chimica Acta* **2004**, *520*, 33-45; i) T. Pihlström, G. Blomkvist, P. Friman, U. Pagard and B. G. Österdahl, *Analytical and Bioanalytical Chemistry* **2007**, *389*, 1773-1789.
[107] a) P. Benigni, C. J. Thompson, M. E. Ridgeway, M. A. Park and F. Fernandez-Lima, *Analytical Chemistry* **2015**, *87*, 4321-4325; b) I. Campuzano, M. F. Bush, C. V. Robinson, C. Beaumont, K. Richardson, H. Kim and H. I. Kim, *Analytical Chemistry* **2012**, *84*, 1026-1033; c) C. Larriba-Andaluz and C. J. Hogan, *Journal of Chemical Physics* **2014**, *141*; d) C. Larriba-Andaluz and J. S. Prell, *International Reviews in Physical Chemistry* **2020**, *39*, 569-623; e) J. F. Maillard, J. Le Maître, C. P. Rüger, M. Ridgeway, C. J. Thompson, B. Paupy, M. Hubert-Roux, M. Park, C. Afonso and P. Giusti, *The Analyst* **2021**, *146*, 4161-4171; f) V. Shrivastav, M. Nahin, C. J. Hogan and C. Larriba-Andaluz, *Journal of the American Society for Mass Spectrometry* **2017**, *28*, 1540-1551.
[108] Z. W. Ulissi, A. J. Medford, T. Bligaard and J. K. Nørskov, *Nature Communications* **2017**, *8*.
[109] J. Boschmans, S. Jacobs, J. P. Williams, M. Palmer, K. Richardson, K. Giles, C. Lapthorn, W. A. Herrebout, F. Lemière and F. Sobott, *Analyst* **2016**, *141*, 4044-4054.
[110] J. N. Dodds, Z. R. Hopkins, D. R. U. Knappe and E. S. Baker, *Analytical Chemistry* **2020**, *92*, 4427-4435.
[111] J. N. Dodds and E. S. Baker, *Journal of the American Society for Mass Spectrometry* **2019**, *30*, 2185-2195.
[112] S. Nekkanti and C. B. Martin, *Pteridines* **2015**, *26*, 13-22.
[113] C. Legault, *Université de Sherbrooke* **2009**, *436*, 437.
[114] a) B. K. Ozgur Golge, *Food Chemistry* **2015**, 319-332; b) L. Zhao and J. Stevens, *LC-GC North America* **2009**, 38-39.

[115] J. C. May, R. Knochenmuss, J. C. Fjeldsted and J. A. McLean, *Analytical Chemistry* **2020**, *92*, 9482-9492.
[116] a) M. S. Díaz-Cruz and D. Barceló, *Journal of Chromatography A* **2006**, *1132*, 21-27; b) Y. Zhang, W. Zhang, X. Liao, J. Zhang, Y. Hou, Z. Xiao, F. Chen and X. Hu, *Ultrasonics Sonochemistry* **2010**, *17*, 662-668.
[117] M. B. Kurade, J. R. Kim, S. P. Govindwar and B.-H. Jeon, *Algal research* **2016**, *20*, 126-134.
[118] N. C.-C. Lidia Belova, Alexander L. N. van Nuijs, and Adrian Covaci, *Analytical Chemistry* **2021**, *93*, 6428-6436.
[119] A. Bauer, J. Kuballa, S. Rohn, E. Jantzen and J. Luetjohann, *Journal of Separation Science* **2018**, *41*, 2178-2187.
[120] N. A. Aly, J. N. Dodds, Y.-S. Luo, F. A. Grimm, M. Foster, I. Rusyn and E. S. Baker, *Analytical and bioanalytical chemistry* **2022**, *414*, 1245-1258.
[121] J. N. Dodds, J. C. May and J. A. McLean, *Analytical Chemistry* **2017**, *89*, 952-959.
[122] K. H. Hendriks, J. J. van Franeker, B. J. Bruijnaers, J. A. Anta, M. M. Wienk and R. A. Janssen, *Journal of Materials Chemistry A* **2017**, *5*, 2346-2354.
[123] W. Zhang and M. L. Wang, *International Journal of Electronics and Electronical Engineering* **2016**, *4*, 177-180.
[124] P. Benigni, R. Marin and F. Fernandez-Lima, *International Journal for Ion Mobility Spectrometry* **2015**, *18*, 151-157.
[125] EPA in *EDSP Weight of Evidence Conclusions on the Tier 1 Screening Assays for the List 1 Chemicals*, *Vol.* Washington, DC, **2015**.
[126] a) T. Benijts, W. Lambert and A. De Leenheer, *Analytical Chemistry* **2004**, *76*, 704-711; b) N. Dujaković, S. Grujić, M. Radišić, T. Vasiljević and M. Laušević, *Analytica Chimica Acta* **2010**, *678*, 63-72; c) W. M. A. Niessen, *Journal of Chromatography A* **2010**, *1217*, 4061-4070; d) G. A. Smith, B. V. Pepich and D. J. Munch, *Journal of Chromatography A* **2008**, *1202*, 138-144; e) M. Mezcua, O. Malato, J. F. Garcia-Reyes, A. Molina-Diaz and A. R. Fernandez-Alba, *Analytical Chemistry* **2009**, *81*, 913-929.
[127] S. Stipičević, G. Mendaš, M. Dvoršćak, S. Fingler, N. Galzina and K. Barić, *Arhiv za Higijenu Rada i Toksikologiju* **2017**, *68*, 336-342.
[128] B. Tariba Lovaković, A. Pizent, V. Kašuba, N. Kopjar, V. Micek, G. Mendaš, M. Dvoršćak, A. Mikolić, M. Milić, S. Žunec, A. Lucić Vrdoljak and D. Želježić, *Food and Chemical Toxicology* **2017**, *108*, 93-103.
[129] M. K. Morgan, L. S. Sheldon, C. W. Croghan, P. A. Jones, G. L. Robertson, J. C. Chuang, N. K. Wilson and C. W. Lyu, *Journal of Exposure Analysis and Environmental Epidemiology* **2005**, *15*, 297-309.
[130] a) A. T. Farag, A. M. El Okazy and A. F. El-Aswed, *Reproductive Toxicology* **2003**, *17*, 203-208; b) J. Flaskos, *Toxicology Letters* **2012**, *209*, 86-93.
[131] J. Hazarika, M. Ganguly and R. Mahanta, *Journal of Applied Toxicology* **2020**, *40*, 434-443.
[132] J. L. Armstrong, R. L. Dills, J. Yu, M. G. Yost and R. A. Fenske, *Journal of Environmental Science and Health - Part B Pesticides, Food Contaminants, and Agricultural Wastes* **2014**, *49*, 102-108.
[133] T. Cáceres, W. He, R. Naidu and M. Megharaj, *Water Research* **2007**, *41*, 4497-4503.
[134] C. Sridevi and G. Velraj, *Spectrochimica Acta Part A: Molecular and Biomolecular Spectroscopy* **2014**, *121*, 533-543.
[135] a) X. L. Lei Fu, Jun Tan, Longxing Wang, Jiping Chen, *Journal of Environmental Sciences* **2018**, 116-125; b) J. Y. L. Nho-Eul Song, Ahmad Rois Mansur, Hae Won Jang, Min-Cheol Lim, Yunyeol Lee, and T. G. N. Miyoung Yoo, *Food chemistry* **2019**, 125050; c) A. Stachniuk, A. Szmagara, R. Czeczko and E. Fornal, *Journal of Environmental Science and Health - Part B Pesticides, Food Contaminants, and Agricultural Wastes* **2017**, *52*, 446-457.

Appendix

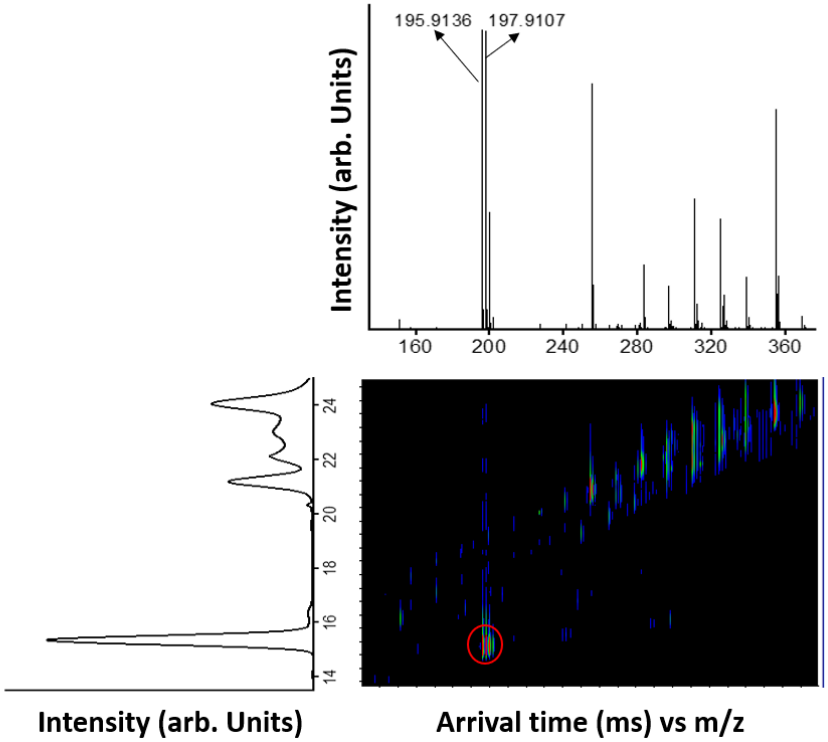

Figure A1: Heat map of pesticide mixture in the negative mode (TCP significantly observed)

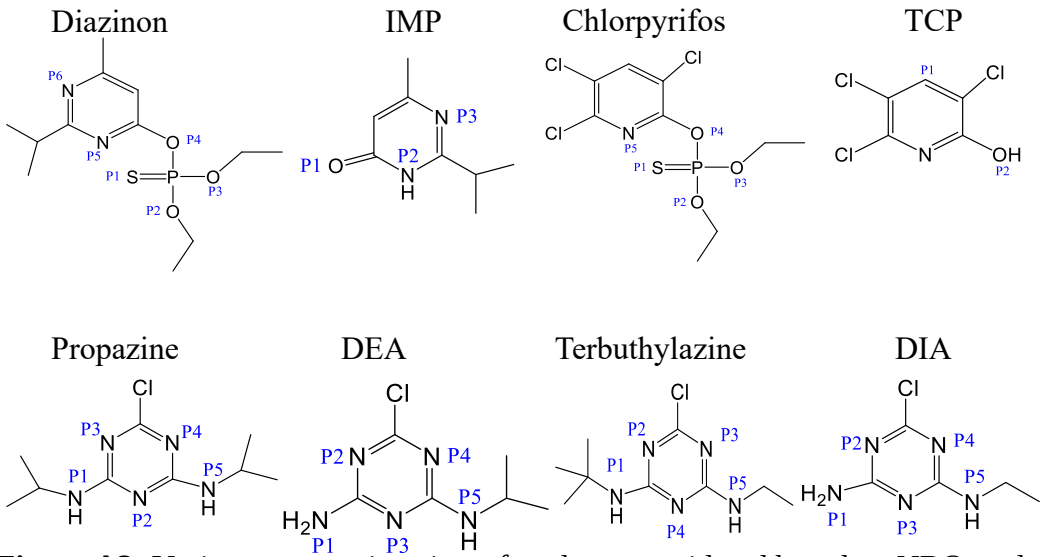

Figure A2: Various protonation sites of analytes considered based on NBO analysis

Propazine

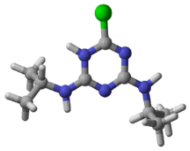

0.0 kcal/mol

CCS – 157.71 Å^2

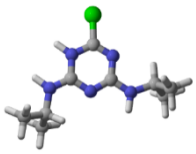

0.4 kcal/mol

CCS – 157.98 Å^2

Atrazine-desethyl

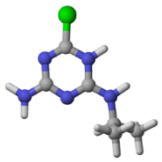

0.0 kcal/mol

CCS – 143.78 Å^2

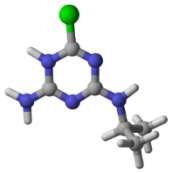

0.4 kcal/mol

CCS – 144.07 Å^2

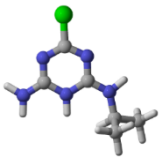

4.9 kcal/mol

CCS – 139.32 Å^2

Chlorpyrifos

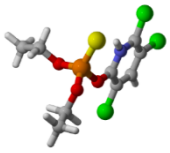

0.0 kcal/mol

CCS – 161.24 Å^2

3,5,6-trichloro-2-pyridinol

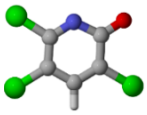

0.0 kcal/mol

CCS – 116.0 Å^2

Terbuthylazine

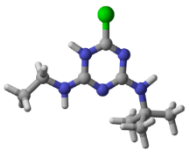

0.0 kcal/mol

CCS – 156.60 Å^2

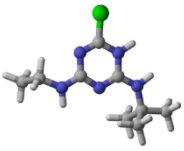

0.6 kcal/mol

CCS – 157.38 Å^2

Atrazine-desisopropyl

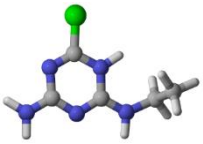

0.0 kcal/mol

CCS – 138.92 Å^2

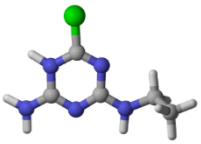

0.6 kcal/mol

CCS – 139.39 Å^2

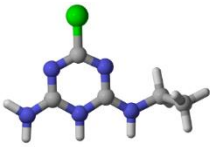

4.9 kcal/mol

CCS – 139.32 Å^2

Diazinon

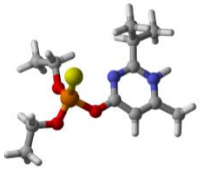

0.0 kcal/mol

CCS – 175.29 Å^2

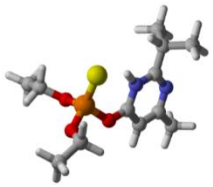

0.2 kcal/mol

CCS – 175.81 Å^2

2-isopropyl-6-methyl-4-pyrimidinol

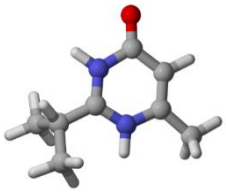

0.0 kcal/mol

CCS – 133.12 Å^2

Figure A3: Stable structures of propazine (2), atrazine-desethyl (3), chlorpyrifos (1), 3,5,6-trichloro-2-pyridinol (1), Terbuthylazine (2), Atrazine-desisopropyl (3), diazinon (2), and 2-isopropyl-6-methyl-4-pyrimidinol (1) with their corresponding relative energies and CCS values.

Table A1: Protonation sites of pesticides and degradation products

Analytes	Protonation site	Relative energy (kcal/mol)
Diazinon	P1	16.82
	P2	8.82
	P3	36.13
	P4	40.43
	P5	0.17
	P6	0.00
2-Isopropyl-6-methyl-4-pyrimidinol	P1	7.90
	P2	42.83
	P3	0.00
Chlorpyrifos	P1	7.17
	P2	23.35
	P3	1.80
	P4	30.52
	P5	0.00
3,5,6-Tricloro-pyridinol	P1	34.6
	P2	0.00
Propazine	P1	18.60
	P2	4.70
	P3	0.39
	P4	0.00
	P5	16.74
Atrazine-desethyl	P1	23.35
	P2	0.36
	P3	4.91
	P4	0.00
	P4	15.43
Terbuthylazine	P1	14.00
	P2	0.62
	P3	0.00
	P4	5.04
	P5	18.36
Atrazine-desisopropyl	P1	22.51
	P2	0.36
	P3	4.95
	P4	0.00
	P5	16.21

Table A2: Comparison of relative energies of protomers of parent pesticides and degradation products at B3LYP/6-31G(d,p) and MP2/6-311++G(d,p) level of theories

Analyte	**Protonation site**	**B3LYP/6-31G(d,p) Relative energy (kcal/mol)**	**MP2/6-311++G(d,p) Relative energy (kcal/mol)**
Diazinon	P5	0.17	0.6
	P6	0.00	0.0
Propazine	P2	4.70	10.79
	P3	0.39	4.52
	P4	0.00	0.00
Atrazine-Desethyl	P2	0.36	0.06
	P3	4.91	6.44
	P4	0.00	0.00
Terbuthylazine	P2	0.62	0.56
	P3	0.00	0.00
	P4	5.04	6.52
Atrazine-Desisopropyl	P2	0.36	0.16
	P3	4.95	6.26
	P4	0.00	0.00